

Crustal motion in Indonesia from Global Positioning System measurements

Y. Bock,¹ L. Prawirodirdjo,¹ J. F. Genrich,¹ C. W. Stevens,² R. McCaffrey,² C. Subarya,³ S. S. O. Puntodewo,³ and E. Calais⁴

Received 25 September 2000; revised 6 March 2003; accepted 14 April 2003; published 6 August 2003.

[1] We present the crustal motion velocity field for the Indonesian archipelago based on Global Positioning System (GPS) field surveys conducted from 1991 to 1997, and 2001, totaling more than 150 sites, as well as on a reanalysis of global tracking data in the Scripps Orbit and Permanent Array Center archive from 1991 to 2001 in International Terrestrial Reference Frame 2000. We compute poles of rotation for the Australia, Eurasia, and Pacific plates based on our analysis of the global GPS data. We find that regional tectonics is dominated by the interaction of four discrete, rotating blocks spanning significant areas of the Sunda Shelf, the South Banda arc, the Bird's Head region of New Guinea, and East Sulawesi. The largest, the Sunda Shelf block (SSH), is estimated to be moving 6 ± 3 mm/yr SE relative to Eurasia. The South Banda block (SBB) rotates clockwise relative to both the SSH and Australia plate, resulting in 15 ± 8 mm/yr of motion across the Timor trough and 60 ± 3 mm/yr of shortening across the Flores Sea. Southern New Guinea forms part of the Australia plate from which the Bird's Head block (BHB) moves rapidly WSW, subducting beneath the Seram trough. The East Sulawesi block rotates clockwise about a nearby axis with respect to the Sunda Shelf, thereby transferring east-west shortening between the Pacific and Eurasia plates into north-south shortening across the North Sulawesi trench. Except for the Sunda Shelf, the crustal blocks are all experiencing significant internal deformation. In this respect, crustal motion in those regions does not fit the microplate tectonics model. *INDEX TERMS:* 1206 Geodesy and Gravity: Crustal movements—interplate (8155); 1243 Geodesy and Gravity: Space geodetic surveys; 8150 Tectonophysics: Plate boundary—general (3040); 8158 Tectonophysics: Plate motions—present and recent (3040); 9320 Information Related to Geographic Region: Asia; *KEYWORDS:* crustal motion, Indonesia tectonics, GPS, current plate motions, Southeast Asia

Citation: Bock, Y., L. Prawirodirdjo, J. F. Genrich, C. W. Stevens, R. McCaffrey, C. Subarya, S. S. O. Puntodewo, and E. Calais, Crustal motion in Indonesia from Global Positioning System measurements, *J. Geophys. Res.*, 108(B8), 2367, doi:10.1029/2001JB000324, 2003.

1. Introduction

[2] The islands of the Indonesian archipelago lie at the junction of the Eurasia, Australia, Pacific, and Philippine Sea plates, resulting in rugged topography, frequent earthquakes, and volcanism [Hamilton, 1979]. In the west, the Australia plate subducts beneath the Eurasia plate along the Java trench while to the east, the continental part of the Australia plate collides with the Banda arc and the Pacific oceanic plate. Recognition of the region's significance to

plate tectonic studies led to a concerted effort, begun in the last decade, to perform Global Positioning System (GPS) geodetic measurements throughout the archipelago. We present the results of these GPS surveys conducted annually from 1991 to 1997, and in 2001, comprising more than 150 stations covering all the major Indonesian islands. The regional tectonics has since been shown to comprise a large variety of phenomena associated with plate convergence: seismogenic subduction zones occurring alongside nonseismogenic ones, partitioning of oblique convergence, forearc deformation, shifting of plate boundaries due to accreting plate margins, and microplate tectonics. Many of these topics are discussed in previous papers that have used subsets of these GPS data [Puntodewo *et al.*, 1994; Tregoning *et al.*, 1994; Genrich *et al.*, 1996, 2000; Prawirodirdjo *et al.*, 1997, 2000; Stevens *et al.*, 1999, 2002; McCaffrey *et al.*, 2000]. This paper centers upon a reanalysis of the entire Indonesia GPS data set in a consistent reference frame, the International Terrestrial Reference Frame ITRF2000 (<http://lareg.ensg.ign.fr/ITRF/ITRF2000/>), includes new data collected in Sumatra in

¹Cecil H. and Ida M. Green Institute of Geophysics and Planetary Physics, Scripps Institution of Oceanography, La Jolla, California, USA.

²Department of Earth and Environmental Sciences, Rensselaer Polytechnic Institute, Troy, New York, USA.

³National Coordination Agency for Surveying and Mapping, Cibinong, Indonesia.

⁴Department of Earth and Atmospheric Sciences, Purdue University, West Lafayette, Indiana, USA.

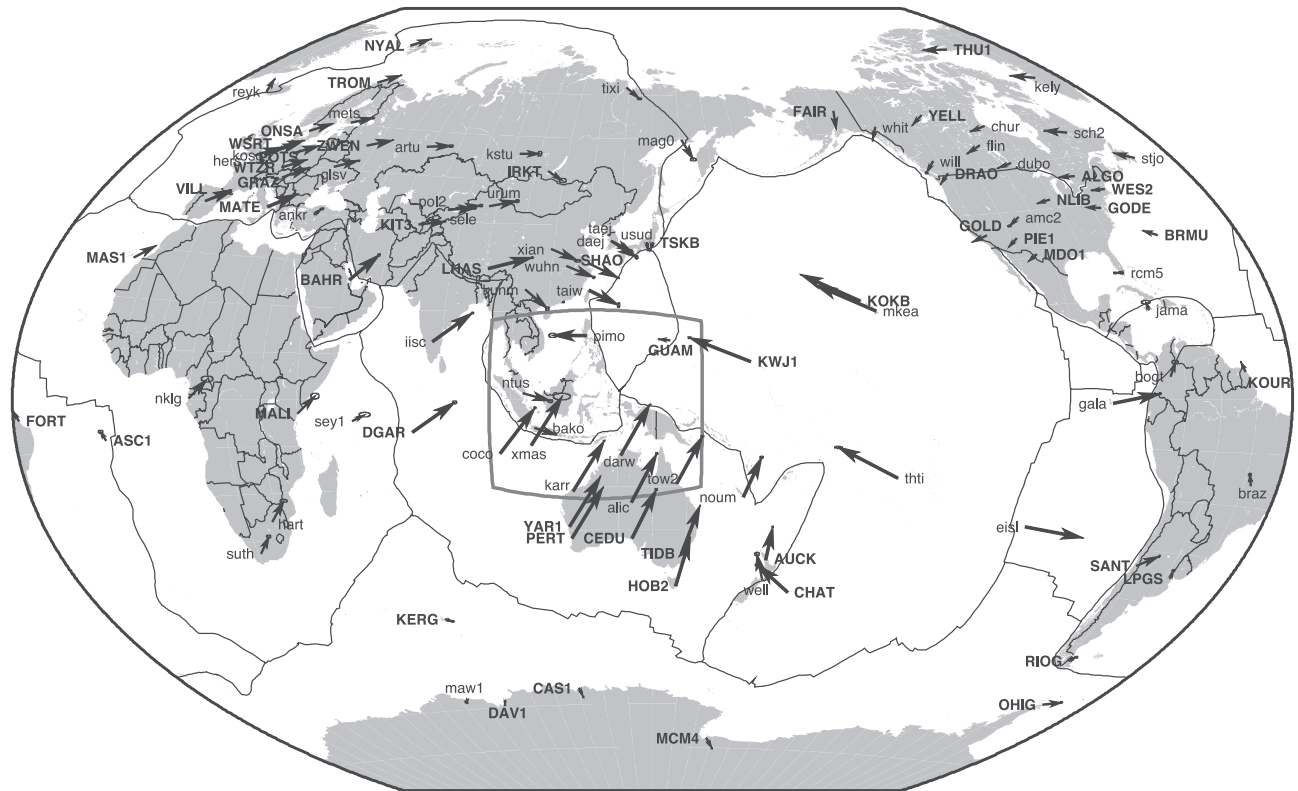


Figure 1. Network of global continuously tracking GPS stations used in processing regional data. Regional data, enclosed by rectangle, are shown in Figure 2. Velocities are in ITRF2000. Stations used for realization of the ITRF2000 reference frame are labeled in bold capital letters. Velocity vector ellipses indicate two-dimensional (2-D) 95% confidence levels based on the formal (white noise only) uncertainty estimates. Stations discussed in the text are included in Table 2 with their velocities and uncertainties.

2001, and makes use of a reanalysis of all global data in the Scripps Orbit and Permanent Array Center (SOPAC) GARNER archive (<http://garner.ucsd.edu/>) since January, 1991 [Bock et al., 2001; Nikolaidis, 2002]. We present a comprehensive horizontal crustal motion velocity field for the global network as well as the survey region (Figure 1). The addition of survey data not analyzed or not yet available in the earlier publications lowers the velocity uncertainties considerably for several stations. Furthermore, the longer time series now available also lowers velocity uncertainties for the global stations, allowing us to better assess the extent of the “rigid” major plates and how our regional survey stations are moving relative to them. In discussing our results, we explore to what extent microplate tectonics can be used as a model for crustal motion in this region. In the context of the “improvements” to our data set, we also recapitulate many of the important results that were first presented in the previous paper listed above.

2. Tectonic Background and Previous Studies

2.1. Western Indonesia

[3] Tectonically, western Indonesia consists of the Sunda Shelf (continental shelf of Southeast Asia), which includes the islands of Sumatra, Java, Bali, Borneo, and the southwestern part of Sulawesi [Hamilton, 1979] (Figure 2). The Sunda Shelf is ostensibly part of the vast Eurasia plate (Figure 3), but the collision of India with central Asia may

cause significant motion of Southeast Asia and the Sunda Shelf relative to Eurasia [Molnar and Tapponnier, 1975; Avouac and Tapponnier, 1993; Chamot-Rooke and Le Pichon, 1999; Michel et al., 2001].

[4] The active tectonics of western Indonesia is dominated by convergence of the Australia plate with Sumatra and Java [Hamilton, 1979]. Along Sumatra the direction of convergence is highly oblique to the trench strike, and is partitioned into nearly arc-perpendicular thrusting at the trench and arc-parallel, right-lateral slip at the Sumatran fault (SF) (Figure 2) [Fitch, 1972; McCaffrey, 1991a; McCaffrey et al., 2000]. Both faults are the source of strong and frequent earthquake activity. Two great ($M > 8$) subduction earthquakes occurred in 1833 and 1861 [Newcomb and McCann, 1987], and several large ($M > 7$) strike-slip events are centered on or near the SF [e.g., Untung et al., 1985]. The partitioning results in the formation of a forearc sliver block between the trench and the SF.

2.2. Eastern Indonesia

[5] Seismic refraction and reflection surveys by Curray et al. [1977] determined that the crustal composition south of Java and Bali and in the south Banda Sea are oceanic, and that the Arafura sea and Timor trough are underlain by continental crust. This, along with the geological evidence of exposed overthrust sheets of the Banda allochthon on the island of Timor [Barber and Audley-Charles, 1976], indicates collision of a continent with an island arc along the

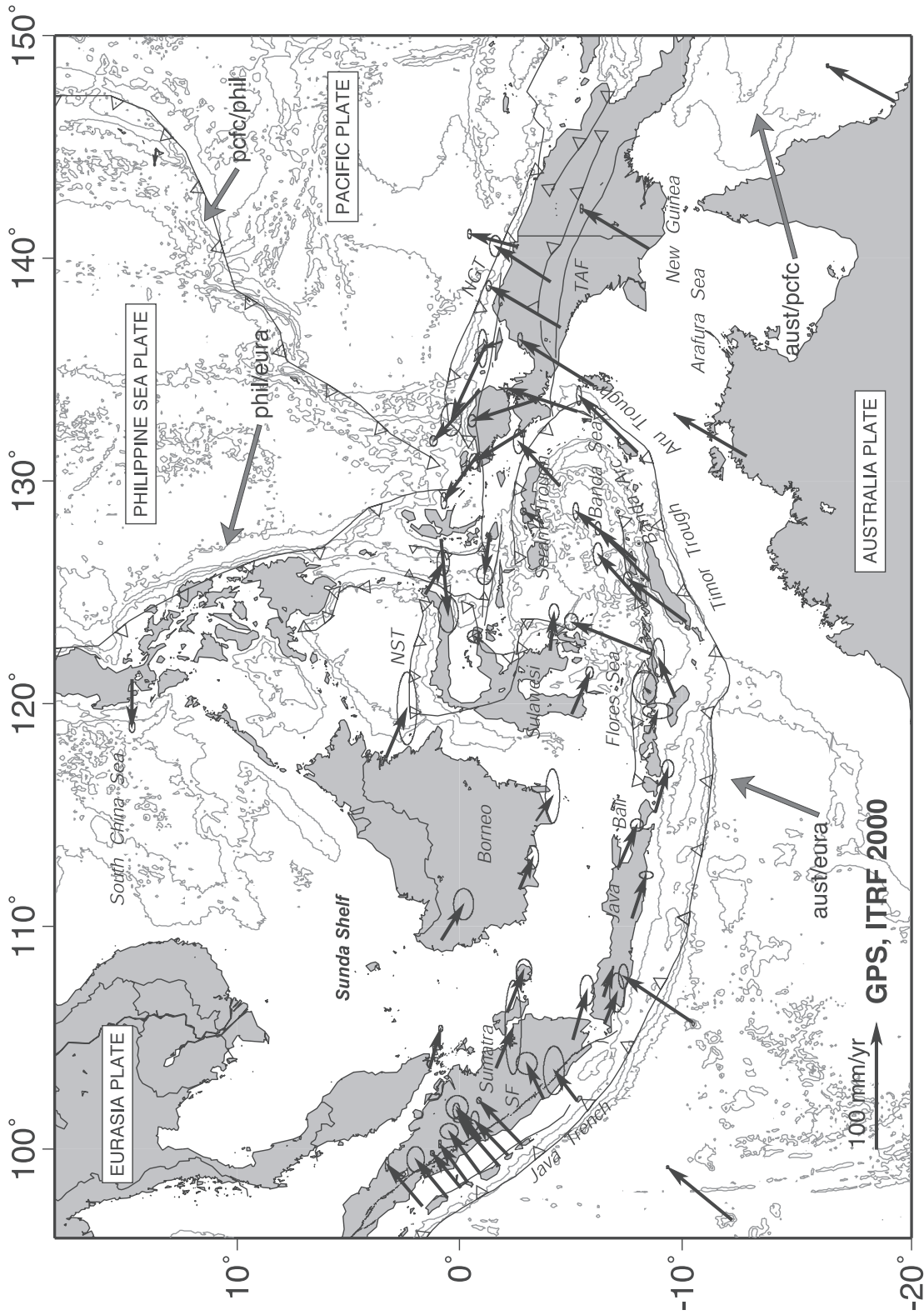


Figure 2. Topographic and tectonic map of the Indonesian archipelago and surrounding region. Labeled, shaded arrows show motion (NUVEL-1A model) of the first-named tectonic plate relative to the second. Solid arrows are velocity vectors derived from GPS surveys from 1991 through 2001, in ITRF2000. For clarity, only a few of the vectors for Sumatra are included. The detailed velocity field for Sumatra is shown in Figure 5. Velocity vector ellipses indicate 2-D 95% confidence levels based on the formal (white noise only) uncertainty estimates. NGT, New Guinea Trench; NST, North Sulawesi Trench; SF, Sumatran Fault; TAF, Tarara-Aiduna Fault. Bathymetry [Smith and Sandwell, 1997] in this and all subsequent figures contoured at 2 km intervals.

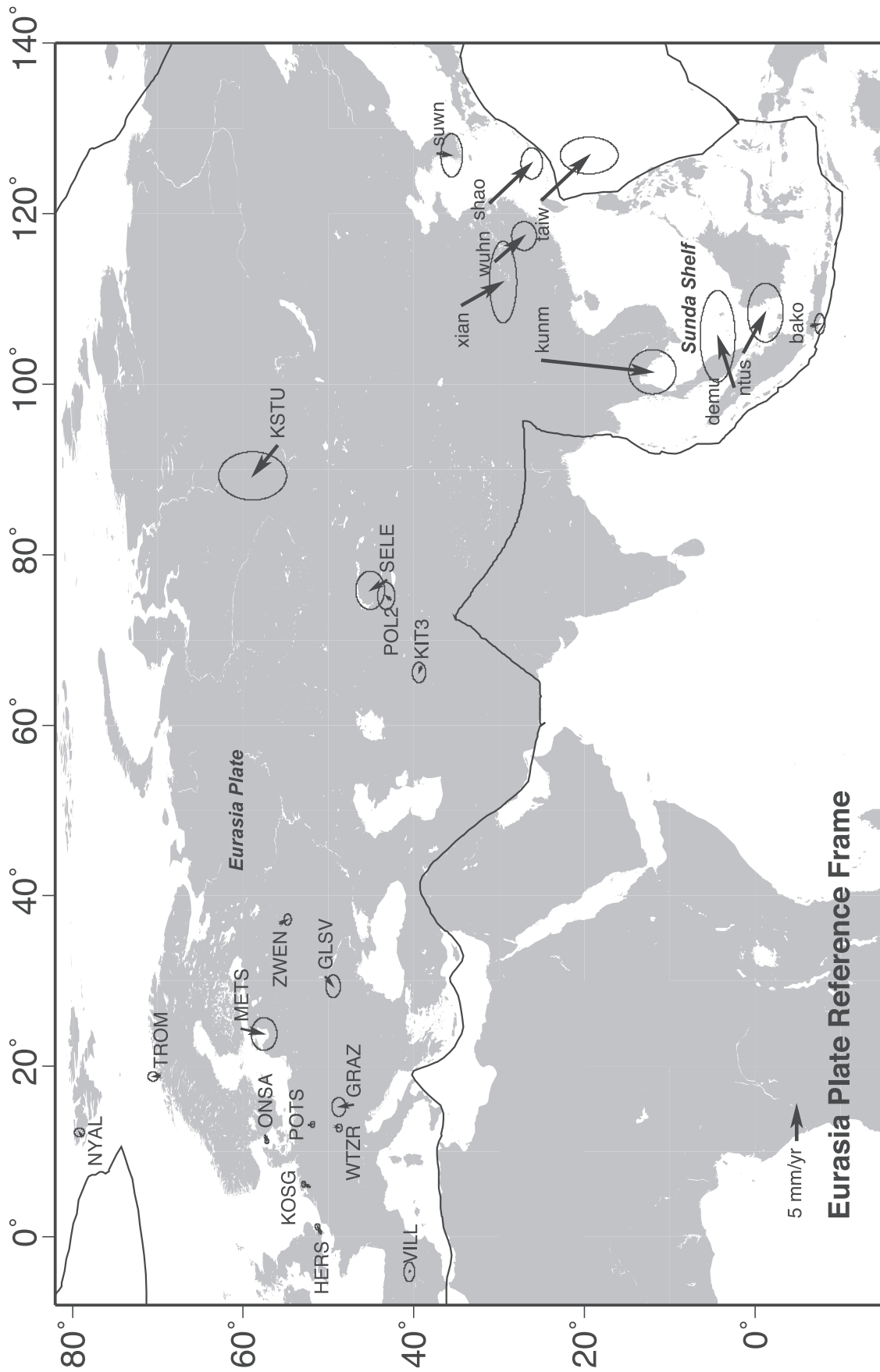


Figure 3. Residual GPS velocity vectors in the estimated Eurasia reference frame (see also Table 2). The 16 sites used to estimate the rotation pole for Eurasia are labeled in capital letters. Ellipses indicate 2-D 95% confidence limits based on the formal (white noise only) uncertainty estimates, scaled by the goodness of fit of the Euler vector estimate (see Table 4).

outer Banda arc, and suggests underthrusting of continental crust under Timor.

[6] *Cardwell and Isacks* [1978] proposed, based on seismicity studies, that two plates subduct beneath the Banda Sea, one from the south at the Timor and Aru troughs, and the other from the north at the Seram trough, and that the two slabs are separated at the Tarera-Aiduna fault (TAF), which acts as a transform (Figure 2). *Jacobson et al.* [1979] used refraction and reflection studies to support the theory that the Timor-Tanimbar-Aru trough system was the surface trace of a subduction zone. Analyses of seismic [McCaffrey and Nabelek, 1984] and geodetic data [Genrich et al., 1996] show only low slip rates at the Timor trough, indicating that subduction is no longer the dominant process accommodating convergence at this boundary. *Abers and McCaffrey* [1988], *McCaffrey* [1988, 1989], and *McCaffrey and Abers* [1991] reinforced the model of *Cardwell and Isacks* [1978] of two separate subducting slabs with evidence from fault plane solutions of earthquakes from the Banda arc and western New Guinea. The Banda basin contracts north-south and extends east-west by strike-slip faulting [McCaffrey, 1988]. The 1978 ($m_b = 5.8$) [McCaffrey and Nabelek, 1984] and 1992 ($M_w = 7.9$) [Beckers and Lay, 1995] earthquakes indicate that some, if not most, of the north-south contraction of the Banda basin is accommodated by active back arc thrusting.

[7] The Australia plate collides obliquely with the oceanic Pacific plate in New Guinea at a rate of 110 mm/yr ENE [DeMets et al., 1994]. A clear result of this convergence is the Highlands thrust belt, a 1000-km-long, 4-km-high, east-west trending mountain belt which covers much of the island. *Abers and McCaffrey* [1988] estimated, from seismic moments and volume of the mountains, that the Highlands thrust belt accounts for only 5–20% of the total convergence. Other candidates for partial accommodation of Pacific-Australia convergence are the New Guinea and Manokwari trenches north of New Guinea. Sonar imagery of the Manokwari trough north of Bird's Head [Milsom et al., 1992] suggests that the trough has recently undergone convergence and transcurrent movement. *Puntodewo et al.* [1994] confirmed, from an analysis of GPS geodetic data, that only about one quarter of Pacific-Australia convergence is accommodated by deformation within New Guinea, implying that rapid subduction must be occurring in the north. They also found little significant slip along the east-west-trending Sorong fault. Recent analysis of GPS measurements and geologic mapping by *Stevens et al.* [2002] indicate that the Bird's Head moves SW relative to Australia at a rate of 80 mm/yr along a shear zone that is up to 300 km wide.

3. Data

3.1. Collection

[8] Our velocity field for Indonesia is based on survey-mode GPS data collected from 1991 to 1994, 1996, 1997, and 2001 at more than 150 sites throughout the archipelago, and global data archived and analyzed by SOPAC since 1991. Survey data collected in 1989 and 1990 were not included in this study because of poor satellite coverage, sparse global data, and GPS selective availability (SA). Table 1 summarizes the occupation history of our survey

campaigns. Over 70 stations are located on Sumatra and the Mentawai islands, and provide dense coverage of the SF and Sumatra subduction zone. Details of the Sumatra surveys are given by *Genrich et al.* [2000] and *Prawirodirdjo et al.* [2000]. GPS surveys in other areas of Indonesia started in western New Guinea in 1991 and spanned all the major islands in Indonesia by 1993. Details of the eastern Indonesia surveys are given by *Stevens* [1999]. In March–May 2001, we resurveyed 26 sites on Sumatra and the Mentawai islands. Although geographically limited, these data allow us to improve the regional reference frame, especially for data collected in the early surveys in western Indonesia.

[9] The 1991 campaign was characterized by limited global data and sparse satellite coverage in Indonesia. The situation improved dramatically with the establishment of the International GPS Service (IGS, <http://igs.cb.jpl.nasa.gov>) in 1992, and the subsequent proliferation of continuous GPS sites, globally as well as regionally. These changes were accompanied by significant improvements in accuracy of the global terrestrial reference frame, maintained by the International Earth Rotation Service (<http://www.iers.org/>), and defined by published site coordinates and velocities. Key reference stations were established in Padang (PADA) in West Sumatra and Cibinong (BAKO) in West Java, and were collected during most annual surveys (Figure 1). Station BAKO became a continuous GPS site and part of the IGS in 1998.

[10] Positions and estimated horizontal velocity components for all sites discussed here are listed in Table 2.

3.2. Processing

[11] Site velocities were estimated using the suite of programs GAMIT version 9.94 [King and Bock, 2000] and GLOBK/GLORG version 5.0 [Herring, 2000]. Although processing of the GPS data from Indonesia had begun upon completion of the first survey in 1989, several improvements to the software and global reference frame in subsequent years prompted a reprocessing of the entire data set with respect to a consistent reference frame, ITRF2000. Furthermore, we made use of a reanalysis of all global data in the SOPAC GARNER archive (<http://garner.ucsd.edu>) since January 1991 [Bock et al., 2001; Nikolaidis, 2002].

[12] For each survey day, dual-frequency carrier phase and pseudorange observations from all sites surveyed concurrently on that day were combined in a weighted least squares adjustment implemented in GAMIT. This analysis produces daily estimates of site coordinates, satellite state vectors, tropospheric zenith delay parameters, and phase ambiguities. Daily solutions for 1991 include data from all available global tracking sites with fairly tight constraints on positions (a few millimeters to a few centimeters, depending on the quality of the station's data) in order to constrain the solution. From 1992 onward, only global stations with satellite visibility concurrent to the regional network (Kokee Park and Pamate in the Pacific, Darwin, Yarragadee, and Canberra in Australia, McMurdo in Antarctica, and Taipei and Usuda in Asia) were included in the daily regional solutions. The remaining global tracking data were included at the next, multiday adjustment stage. All the global GPS stations used in this study are listed in Table 3 and Figure 1.

[13] The daily regional solutions were then combined, using GLOBK, with daily solutions from global tracking

Table 1. Days Per Year of Occupation for Regional Campaign Stations Used in This Analysis

Site	1991	1992	1993	1994	1996	1997	2001	Span ^a
AIRB	10	...	5	3	10
AJUN	10	...	5	3	10
AMBG	...	4	...	22	7	8	...	5
ARUX	...	6	3	...	5
AUKE	3	5	9	3	...	7	...	6
BANJ	...	8	...	3	2
BAPI	...	3	...	2	2
BIAK	1	5	4	3	3
BIMA	...	5	4	4	2
BINA	10	...	2	4
BINT	2	...	3	3	10
BLMS	17	...	11	4
BPIL	...	2	5	4	2
CINA	...	2	4	3	2
D937	3	...	4	2	10
D944	7	...	11	3	10
D947	5	...	6	3	10
D949	3	...	4	3	10
D952	7	...	4	1	10
D953	3	...	4	3	10
D956	10	...	5	3	10
D957	3	...	4	2
D962	3	...	5	3	10
D967	3	...	4	2
D970	3	...	4	2
D972	2	...	5	2
DARW	...	44	51	8	27	9
DEMP	...	4	...	3	2
DEMU	11	...	5	3	10
DENP	...	8	7	4	5
DILI	...	14	...	4	2
DOLO	2	4
DURI	26	...	11	2
ENGG	...	3	4	2	2
FAKF	...	9	3	6	4	4
JAMB	...	4	3	3	2
JOGY	...	3	...	3	2
JULU	7	...	2	3	10
KACA	3	...	5	3	10
KAIM	...	12	4	5	6	4
KALA	...	3	9	8	2
KALP	...	2	...	5	2
KAYA	...	6	6	3	2
KEND	...	13	3	10	2
KRUI	...	2	5	4	2
KULU	...	8	2	3	2
KUPA	...	9	19	10	2
LAKO	4	...	8	2
LUWU	...	11	...	11	2
MANA	...	12	...	13	2
MANO	...	4	6	3	2
MART	3	...	6	...	3	...	3	10
NSIB	4	...	4	5	10
OBIX	...	7	...	7	2
P001	4	...	5	2
P002	3	...	4	2
P003	5	3	8
P004	4	...	5	2
P005	4	...	4	2
P007	4	...	5	2
P008	4	...	5	2
P015	4	...	4	2
P016	4	...	4	2
P051	2	...	3	2
P061	4	4
P37E	3	...	9	3	10
PADA	11	11	12	4	11	...	4	10
PADU	2	...	33	5
PAGA	...	3	4	...	5	...	5	9
PALE	...	2	4	1
PAND	5	...	2	3	10

Table 1. (continued)

Site	1991	1992	1993	1994	1996	1997	2001	Span ^a
PANG	...	2	...	11	2
PANT	2	...	3	4
PASI	10	...	5	4
PAUH	4	...	3	4
PETO	4	...	4	4
PISA	5	...	3	3	10
RUMB	10	...	22	4
RUTE	...	5	8	1
SAUM	...	15	...	7	2
SENT	3	4	8	2	4	4	...	6
SIBI	3	...	3	4
SIGL	3	...	2	4
SIKA	9	...	9	2	10
SIOB	3	...	4	5
SIPA	4	...	9	4
SORO	2	12	3	6	4	5
SPG2	5	1	...	3	10
SURA	...	5	...	4	2
TANJ	10	...	5	4
TARA	...	9	...	6	2
TERN	...	4	...	8	2
TIMI	6	15	5	6	3	5
TOBO	4	...	6	3	10
TOWN	38	55	9	2
TUAL	...	14	3	...	5
UJUN	...	20	15	16	2
ULUA	3	2
WAIN	...	2	4	5	2
WAME	2	5	4	2	3	4	...	6
WETA	...	9	...	2	2
XMAS	11	1	12	9	5
YAPE	...	4	3	4	2

^aTime span in years of each time series.

sites provided by the IGS (<http://igs.cb.jpl.nasa.gov/>), this time with loose constraints applied to all station, satellite, and Earth orientation parameters (EOP). The result is a loosely constrained position time series for the entire survey span. To obtain station coordinates in the ITRF2000, we performed an adjustment, using GLORG, constraining the ITRF2000 coordinates and velocities of appropriate global tracking sites that comprise the reference network. The reference stations, which were constrained to their ITRF2000 values, are listed in bold letters in Table 3 and Figure 1. Velocities were then estimated using a weighted least squares line fit to the daily position time series, including offset parameters for sudden site motion due to earthquakes and monument changes [Nikolaidis, 2002].

3.3. Uncertainties Assessment

[14] To assess the accuracy of GPS-based site positions and velocities, daily and long-term baseline repeatabilities were examined from a number of surveys with the method of Larson and Agnew [1991]. Since 1992, with the implementation of the IGS network, daily root-mean-square RMS baseline repeatabilities have been 2–4 mm for the north, 4–6 mm for the east, and 10–15 mm for the vertical component. Uncertainties in the horizontal velocities listed in Table 2 are the formal 1σ standard deviations. These formal standard deviations are typically about 2 mm/yr in the north and 4 mm/yr in the east component for sites whose observations span 6 years or less. For sites with observations spanning 10 years or more, the standard deviations are about half as large or better, assuming a white noise stochastic model for site coordinates.

Table 2. Station Coordinates, Observed ITRF2000 Velocities, 1 σ Uncertainties, and Residuals^a

Site Code	Longitude, °E	Latitude, °N	ITRF2000, mm/yr				Residual, mm/yr ^b	
			V_e	V_n	σ_{V_e}	σ_{V_n}	V_e	V_n
<i>Australia Plate</i>								
ALIC	133.8855	-23.6701	29.5	55.2	0.6	0.4	-2.4	-2.1
AUCK	174.8344	-36.6028	3.0	37.5	0.4	0.3	-2.1	-2.0
CEDU	133.8098	-31.8667	28.6	54.8	0.5	0.4	-0.2	-2.5
COCO	96.8340	-12.1883	41.8	51.0	0.5	0.3	-1.2	1.7
DARW	131.1327	-12.8437	33.3	57.3	0.4	0.1	-2.6	-0.2
HOB2	147.4387	-42.8047	14.4	54.2	0.2	0.1	-0.1	-0.2
KARR	117.0972	-20.9814	38.0	56.7	0.4	0.2	-0.9	0.1
NOUM	166.4102	-22.2699	17.9	44.8	0.7	0.5	-3.2	-0.4
PERT	115.8852	-31.8020	39.4	57.0	0.2	0.1	1.2	0.7
TIDB	148.9800	-35.3992	18.9	54.0	0.1	0.1	0.3	0.2
TOW2	147.0557	-19.2693	28.3	53.3	0.7	0.4	-0.9	-1.2
YAR1	115.3470	-29.0466	39.0	56.0	0.1	0.1	0.1	-0.2
Arux	134.3120	-5.9874	36.2	58.4	2.3	0.8	-0.4	1.1
Auke	140.4141	-8.4671	32.2	53.8	1.5	0.5	-3.1	-2.5
Timi	136.8952	-4.5033	33.2	57.1	1.7	0.8	-3.5	0.2
Xmas	105.6896	-10.4496	36.7	54.9	4.0	1.6	-4.2	1.7
<i>Eurasia Plate</i>								
GLSV	30.4967	50.3642	21.7	11.0	0.4	0.3	-1.3	-1.1
GRAZ	15.4935	47.0671	20.9	16.2	0.3	0.3	-0.3	2.1
HERS	0.3363	50.8673	18.2	15.7	0.1	0.1	1.0	0.5
KIT3	66.8854	39.1348	27.7	4.5	0.4	0.2	-0.9	0.3
KOSG	5.8096	52.1784	18.4	15.8	0.1	0.1	0.4	0.9
KSTU	92.7938	55.9932	22.0	0.9	0.9	1.2	-4.3	3.5
METS	24.3953	60.2175	18.5	9.8	0.6	0.5	-0.7	-3.3
NYAL	11.8651	78.9296	10.1	14.8	0.2	0.2	0.5	0.3
ONSA	11.9255	57.3953	16.7	14.2	0.1	0.1	-0.9	-0.2
POL2	74.6943	42.6798	29.0	2.8	0.5	0.3	0.6	0.7
POTS	13.0661	52.3793	19.5	13.7	0.1	0.1	0.2	-0.6
SELE	77.0169	43.1787	27.0	3.9	0.7	0.5	-1.5	2.3
TROM	18.9383	69.6627	14.8	14.8	0.2	0.2	-0.2	1.1
VILL	-3.9520	40.4436	19.2	15.4	0.3	0.2	-0.2	0.1
WTZR	12.8789	49.1442	20.1	13.9	0.1	0.1	-0.1	-0.5
ZWEN	36.7586	55.6993	23.3	9.9	0.2	0.1	0.6	-1.1
Bako	106.8489	-6.4911	23.3	-7.5	0.4	0.2	0.3	-1.3
Banj	114.7548	-3.4238	19.5	-13.2	8.8	2.3	-4.5	-5.1
Demu	99.6288	2.4623	32.6	-2.1	1.6	0.6	7.3	2.3
Denp	115.1515	-8.7600	34.4	-10.0	2.9	1.9	11.9	-1.8
Jogy	110.3768	-7.7224	34.2	-11.3	1.2	2.2	11.5	-4.2
Kalp	106.1404	-2.1476	33.6	-13.1	3.6	2.6	9.3	-7.1
Kaya	109.4117	0.8067	28.1	-17.4	5.1	3.3	3.1	-10.6
Ntus	103.6800	1.3458	30.8	-8.6	1.1	0.6	5.7	-3.1
Pang	111.6701	-2.6863	25.5	-10.8	3.9	1.8	1.4	-3.4
Shao	121.2004	31.0996	33.1	-15.5	0.6	0.4	5.7	-6.0
Sura	112.6642	-7.1180	33.4	-14.6	2.0	2.1	10.5	-7.0
Taiw	121.5365	25.0213	33.9	-16.3	0.7	1.0	6.4	-6.8
Tara	117.5701	3.3046	39.4	-16.7	11.8	3.2	13.9	-8.0
Wuhn	114.3573	30.5317	31.6	-12.2	0.5	0.5	3.7	-4.2
Xian	109.2215	34.3687	31.5	-12.7	1.5	0.5	3.3	-5.9
<i>Pacific Plate</i>								
CHAT	-176.5658	-43.9558	-40.5	30.5	1.0	0.5	1.8	0.4
KOKB	-159.6649	22.1263	-62.6	31.6	0.3	0.1	0.0	0.2
KWJ1	167.7302	8.7222	-68.3	27.2	0.7	0.5	1.1	0.7
MKEA	-155.4563	19.8014	-64.1	31.1	0.4	0.3	-1.3	-0.3
THTI	-149.6064	-17.5771	-71.4	33.7	1.8	0.4	-5.3	2.8
<i>Sunda Shelf Block</i>								
BAKO	106.8489	-6.4911	23.3	-7.5	0.4	0.2	-1.2	1.4
BANJ	114.7548	-3.4238	19.5	-13.2	8.8	2.3	-6.3	-1.4
DEMU	99.6288	2.4623	32.6	-2.1	1.6	0.6	4.7	4.1
DENP	115.1515	-8.7600	34.4	-10.0	2.9	1.9	10.7	2.0
JOGY	110.3768	-7.7224	34.2	-11.3	1.2	2.2	10.2	-1.0
KALP	106.1404	-2.1476	33.6	-13.1	3.6	2.6	7.3	-4.4
KAYA	109.4117	0.8067	28.1	-17.4	5.1	3.3	0.8	-7.6
NTUS	103.6800	1.3458	30.8	-8.6	1.1	0.6	3.3	-0.8
PANG	111.6701	-2.6863	25.5	-10.8	3.9	1.8	-0.6	-0.1
SHAO	121.2004	31.0996	33.1	-15.5	0.6	0.4	0.4	-1.5
SURA	112.6642	-7.1180	33.4	-14.6	2.0	2.1	9.1	-3.6

Table 2. (continued)

Site Code	Longitude, °E	Latitude, °N	ITRF2000, mm/yr				Residual, mm/yr ^b	
			V_e	V_n	σ_{V_e}	σ_{V_n}	V_e	V_n
TAIW	121.5365	25.0213	33.9	-16.3	0.7	1.0	1.6	-2.3
TARA	117.5701	3.3046	39.4	-16.7	11.8	3.2	11.3	-4.0
UJUN	119.5488	-5.0262	32.9	-14.3	1.9	1.2	7.6	-0.8
WUHN	114.3573	30.5317	31.6	-12.2	0.5	0.5	-1.8	-0.5
XIAN	109.2215	34.3687	31.5	-12.7	1.5	0.5	-2.6	-2.9
Airb	99.3879	0.2211	24.9	11.8	1.4	0.9	-2.2	17.9
Ajun	99.7655	-0.1573	26.6	16.5	1.6	0.8	-0.4	22.8
Bint	98.1779	1.4689	40.6	19.8	2.9	0.9	12.9	25.4
Blms	100.7599	1.6526	54.2	-11.6	4.9	5.5	26.6	-4.9
Bpil	105.6385	-6.4886	24.8	-9.9	6.4	2.4	0.3	-1.4
D937	99.2781	-1.7349	36.3	31.4	0.8	1.8	9.9	37.4
D944	98.5261	0.3406	30.2	21.8	1.3	0.4	3.3	27.6
D947	98.8460	0.0854	33.0	6.2	2.8	1.5	5.9	12.1
D949	98.2744	-0.0353	27.5	22.5	0.9	0.6	0.4	28.2
D952	97.8185	0.5587	30.6	25.2	4.2	2.8	3.3	30.7
D953	97.9456	0.9582	31.7	22.9	0.9	0.6	4.3	28.4
D962	97.4465	1.6860	33.1	28.1	2.3	0.5	5.4	33.4
Duri	101.2194	1.2224	44.8	-5.5	4.6	5.7	17.3	1.3
Engg	102.1638	-5.2562	24.3	18.3	7.9	3.4	-0.6	25.5
Jamb	103.6448	-1.6288	32.4	-13.7	15.3	2.6	6.0	-5.9
Julu	98.4588	2.1219	28.8	14.3	1.6	1.3	0.9	20.0
Kaca	100.6526	-0.7008	33.3	4.5	0.6	0.6	6.6	11.1
Kalp	106.1404	-2.1476	33.6	-13.1	3.6	2.6	7.3	-4.4
Kend	122.4075	-4.0604	30.0	-3.1	2.8	1.6	4.3	11.3
Kulu	102.2531	-3.7599	28.4	13.4	3.6	3.4	2.8	20.6
Kunm	102.7970	24.8824	26.9	-21.0	0.8	0.8	-6.9	-13.6
Luwu	122.7721	-1.0335	4.3	6.5	2.0	2.3	-22.4	21.0
Mana	124.9247	1.5365	25.0	-14.1	4.2	2.0	-2.5	1.1
Mart	98.6823	2.5242	28.6	7.0	2.3	0.8	0.6	12.9
Nsib	98.9095	-0.9154	33.5	24.7	2.5	3.0	6.8	30.6
P003	100.4293	-1.1092	28.0	20.3	2.0	1.2	1.4	26.8
P37e	99.8591	0.6203	28.4	5.0	0.7	0.4	1.1	11.3
Pada	100.3692	-0.9438	28.0	16.3	0.6	0.5	1.3	22.8
Padu	100.3531	-0.8784	24.5	18.3	2.4	1.1	-2.2	24.7
Paga	100.2150	-2.7584	34.9	33.7	1.0	0.7	9.0	40.1
Pand	98.8188	1.6759	21.8	15.2	3.5	1.6	-5.9	21.1
Pasi	100.3692	0.8383	44.8	5.1	9.1	6.6	17.4	11.6
Pisa	98.9068	1.8515	28.0	14.3	1.1	1.0	0.2	20.2
Sika	99.0838	0.6379	25.3	14.1	0.8	0.7	-2.0	20.1
Siob	99.7323	-2.1710	27.4	26.4	3.1	1.3	1.2	32.7
Sp2	100.4487	-0.9420	25.2	18.8	3.9	3.6	-1.4	25.3
Tobo	100.1628	-0.6214	29.1	15.5	0.8	0.5	2.3	21.9
<i>South Banda Block</i>								
DILI	125.5281	-8.4914	41.6	41.2	2.2	0.9	4.5	-3.4
KALA	124.5955	-8.0818	37.7	33.9	3.7	1.5	-1.1	-14.2
KUPA	123.6631	-10.1104	34.1	46.5	2.4	1.4	3.3	-5.2
MAUM	122.2370	-8.5800	25.6	64.1	2.7	2.2	-11.5	7.1
WETA	126.4286	-7.8823	39.4	47.9	2.8	0.9	0.0	6.8
Ambg	128.0889	-3.6827	9.6	14.6	1.1	0.9	-46.4	-20.0
Bapi	129.7754	-4.4895	35.5	33.0	4.0	1.7	-17.3	4.8
Bima	118.6928	-8.4871	17.4	-6.7	2.5	4.9	-20.6	-77.0
Rute	120.4784	-8.5403	4.4	4.9	5.5	4.0	-33.1	-58.8
Saum	131.3069	-7.9361	45.0	46.4	3.1	0.8	6.2	24.2
Tual	133.1250	-5.2511	18.7	56.7	1.4	0.7	-30.9	41.6
Wain	120.3014	-9.6059	31.3	13.1	6.3	2.1	-2.1	-51.2
<i>Bird's Head Block</i>								
BIAK	136.0899	-1.1599	-30.2	91.8	6.9	6.7	-18.4	-19.1
FAKF	132.2647	-2.8998	-24.7	39.7	2.5	1.7	1.9	5.8
KAIM	133.6943	-3.6202	-17.6	54.6				

Table 3. Global, Continuously Tracking Stations Used in Processing 1991–2001 GPS Data From Indonesia^a

Code	Location	1991	1992	1993	1994	1996	1997	2001
ALGO	Algonquin, Canada		•	•	•	•	•	
AREQ	Arequipa, Peru						•	
AUCK	Auckland, New Zealand					•	•	•
AUSA	Adelaide, Australia							
BAHA	Bahrain						•	
BRAZ	Brasilia, Brazil						•	
BRMU	Bermuda						•	
CAS1	Casey, Antarctica			•	•		•	
CHAT	Chatham Island						•	
DARW	Darwin, Australia		•	•				
DAV1	Davis, Antarctica						•	
DRAO	Penticton, Canada	•	•	•	•	•		•
DS10	Goldstone, California	•	•	•	•			
DS40	Canberra, Australia	•						
MADR	Madrid, Spain	•	•	•	•			
ENGA	England							
FAIR	Fairbanks, Alaska		•			•	•	
FORT	Fortaleza, Brazil			•	•	•	•	•
GODE	Greenbelt, Maryland					•	•	•
GOL2	Goldstone, California					•	•	
GUAM	Guam					•	•	•
HART	Hartbeesthoek, S. Africa		•	•	•			
HARK	Hartbeesthoek, S. Africa							
HERS	Herstmonceux, UK		•	•	•			
HOB2	Hobart, Tasmania					•	•	•
KERG	Kerguelen Islands					•	•	•
KIT3	Kitab, Uzbekistan					•		
KOKE	Kokee Park, Hawaii	•						
KOKB	Kokee Park, Hawaii		•	•	•			
KOKR	Kokee Park, Hawaii					•		
KOSG	Kootwijk, Netherlands		•	•	•	•	•	
KOUR	Kourou, French Guyana		•	•	•			
KWAJ	Kwajalein, Marshall Is.	•						
KWJ1	Kwajalein, Marshall Is.					•	•	•
LHAS	Lhasa, Tibet						•	
MAC1	MacQuarie Island						•	
MALI	Malindi, Kenya						•	
MAS1	Maspalomas, Spain					•	•	•
MATE	Matera, Italy						•	
MCM1	McMurdo, Antarctica		•	•	•		•	
MCM4	McMurdo, Antarctica							•
MOJ1	Mojave, California	•						
NYAL	Ny-Alesund, Norway		•	•	•		•	
ONSA	Onsala, Sweden	•	•	•	•	•	•	
PAMA	Pamate, Tahiti		•	•	•			
PERT	Perth, Australia			•	•	•	•	
PIE1	Pie Town, New Mexico					•		•
POTS	Potsdam, Germany					•	•	•
RIC1	Richmond, Florida	•						
RCM5	Richmond, Florida				•			
S01R	Taipei, Taiwan	•						
SANT	Santiago, Chile		•	•	•		•	
STJO	St. John's, Canada		•	•	•			
TAIW	Taipei, Taiwan		•	•	•			
THUI	Thule, Greenland					•	•	•
TIDB	Tidbinbilla, Australia		•	•	•		•	
TOWN	Townsville, Australia	•	•	•	•			
TROM	Tromso, Norway		•	•	•	•		
TSU1	Tsukuba, Japan	•						
TSKB	Tsukuba, Japan					•	•	
USUD	Usuda, Japan		•	•			•	
VILL	Villafranca, Spain							
WAUS	W. Australia							
WELL	Wellington, New Zealand	•						
WES1	Westford, Massachusetts	•						
WES2	Westford, Massachusetts			•	•	•		
WSRT	Westerbork, Netherlands							•
WTZM	Wetzell, Germany	•						
WTZR	Wetzell, Germany		•	•	•	•	•	•
YAR1	Yarragadee, Australia		•	•	•	•	•	•
YELL	Yellowknife, Canada	•	•	•	•		•	
ZWEN	Zwenigorod, Russia					•	•	•

^aSite codes in boldface identify sites used to impose ITRF2000 reference frame.

[15] Time series analyses of continuous GPS data in southern California by *Bock et al.* [1997] and *Zhang et al.* [1997] suggest that GPS position estimates contain significant colored noise. If a similar noise spectrum applies to our station positions, our velocity uncertainties would be 2–4 times larger than uncertainties obtained assuming a purely white noise model. We tested this hypothesis for our data set by applying a white noise plus flicker noise model, as described by *Nikolaidis* [2002], to the Indonesia survey stations. We assumed a uniform noise amplitude for all stations based on the values for site BAKO on Java, which was estimated by analyzing [*Williams*, 2003] the full continuous BAKO time series (<http://sopac.ucsd.edu/>). We found that for stations with daily repeatabilities similar to BAKO, as with BAKO itself, the velocity uncertainties increased by a factor of two compared to when we assumed a white noise model. For a few survey stations with scatter much larger than that of BAKO and with only two observation campaigns, assumption of the same noise model yielded anomalous results, and is clearly not appropriate. Nevertheless, to maintain a uniform approach for all stations, we retained the white noise assumption for all stations but applied a factor of two when using the formal uncertainties to weight the velocities for estimation of Euler vectors and strain rates. That is, the GPS vectors were weighted by $(2\sigma)^{-2}$, with the exception of the Australia stations (as noted in section 6.1).

[16] Velocity vectors with respect to ITRF2000 are drawn in Figures 1 and 2 with 2-D 95% confidence limits based on the formal (white noise only) uncertainty estimates. Residual velocity vectors with respect to the estimated poles of rotation are drawn in Figures 3–8 with 2-D 95% confidence limits based on the formal (white noise only) uncertainty estimates, but scaled by the goodness of fit of the corresponding pole estimate (see Table 4).

4. ITRF2000 Velocity Field

[17] Velocities derived from our GPS surveys in Indonesia are plotted in Figure 2 in ITRF2000. The velocity field clearly shows several distinct tectonic regimes: The Sunda Shelf moves ESE, the southern Banda arc and southern New Guinea moves NE and NNE, and the Bird's Head region (NW New Guinea) moves NW, with velocities directed NW. Smaller tectonic units include the Sumatra forearc (the islands SW of Sumatra) and northeastern Sulawesi [as identified by *Stevens et al.*, 1999].

[18] To quantify the regional motions relative to the major tectonic plates, we estimate rotation parameters for the Eurasia, Australia, and Pacific plates (Table 4), as well as for the regional crustal blocks mentioned above. In the following sections, we discuss the regional kinematics and deformation in terms of the motions of the regional blocks relative to the three major plates. We also estimate strain rates for various blocks (Table 5) by fitting the GPS velocities to a deformation rate gradient tensor as described by *McCaffrey et al.* [2000].

5. Motion Relative to Eurasia

5.1. Eurasia Pole of Rotation

[19] We compute rotation parameters for Eurasia by minimizing the velocities of 12 stations in Europe and 4

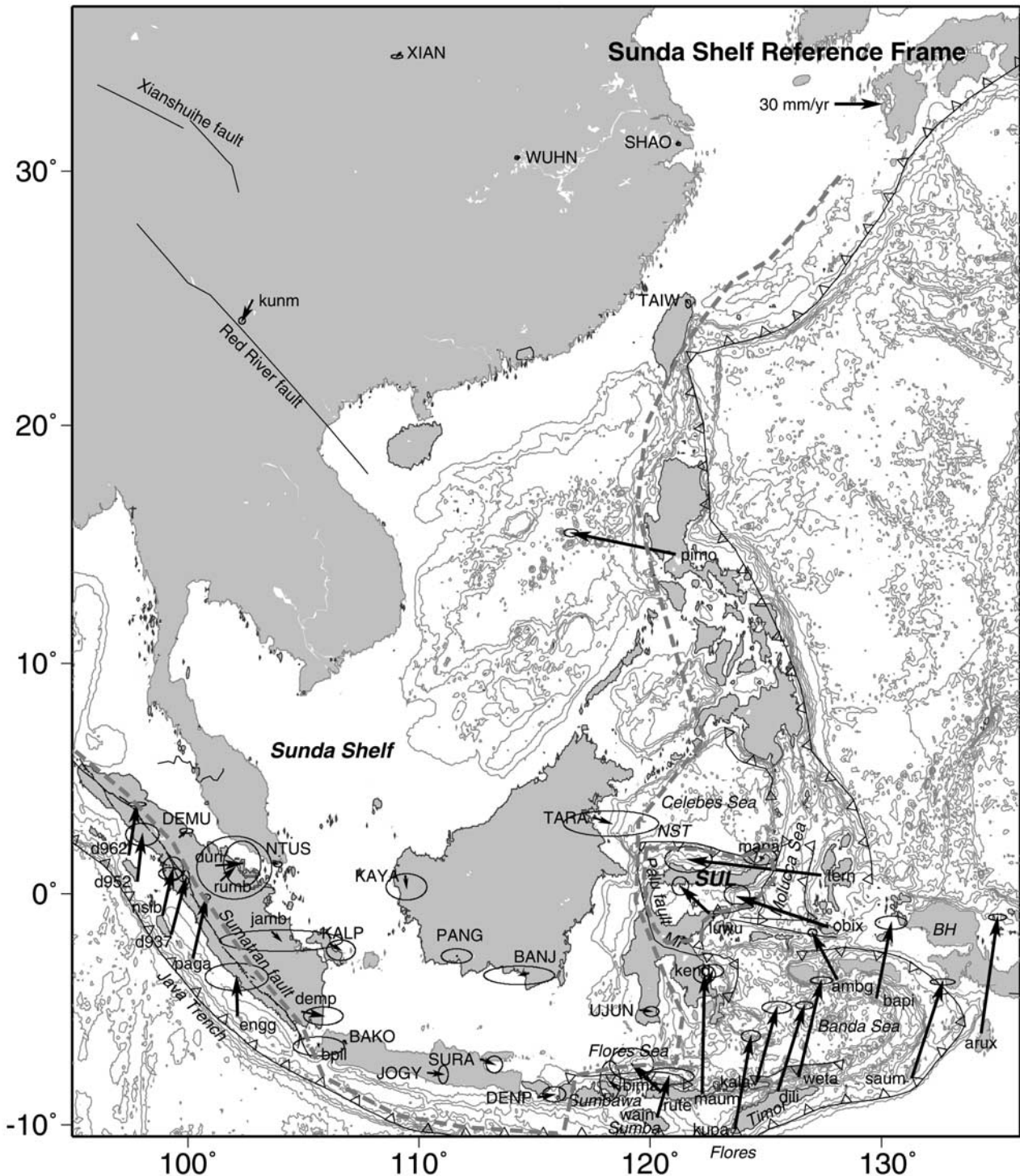


Figure 4. GPS velocity vectors in the estimated Sunda Shelf reference frame (see also Table 2). Some stations on Sumatra have been omitted to preserve clarity, but can be viewed in Figure 5. Heavy dashed lines indicate crustal block boundaries. SUL, East Sulawesi block; BH, Bird's Head; NST, North Sulawesi Trench. The 16 sites used to estimate the rotation pole for the SSH are labeled in capital letters. Ellipses indicate 2-D 95% confidence limits based on the formal (white noise only) uncertainty estimates, scaled by the goodness of fit of the Euler vector estimate (see Table 4).

stations in central Asia (Table 2 and Figure 3). The resulting Euler vector is consistent, within the uncertainties, with the Eurasia pole computed by *Larson et al.* [1997] and *Sella et al.* [2002] (Table 4). The mean residual speed for the

Eurasia plate stations (Table 2 and Figure 3) is 1.5 ± 1.4 mm/yr.

[20] The Sunda Shelf is postulated to be the largest present-day tectonic block in Indonesia [*Genrich et al.*,

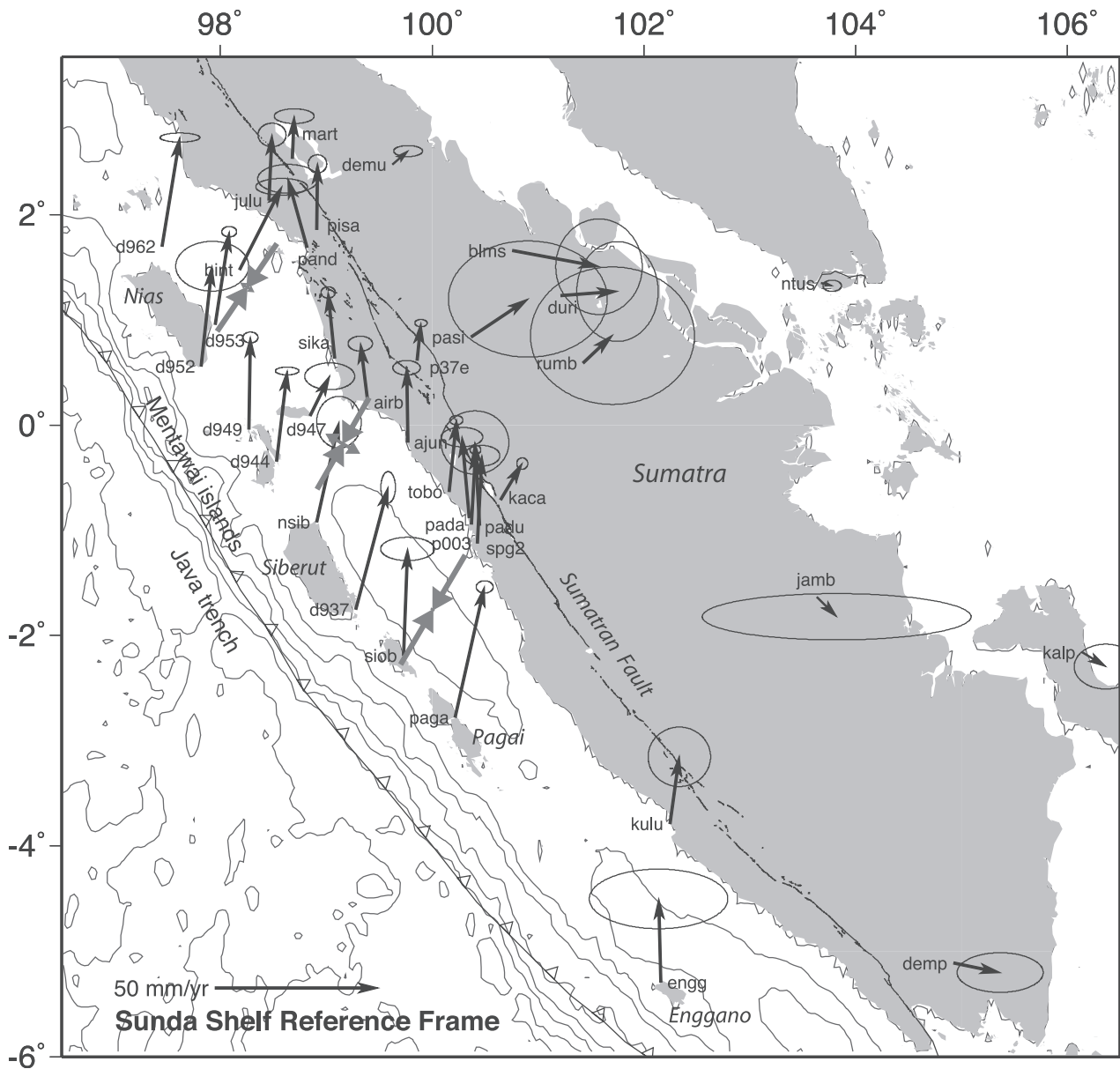


Figure 5. GPS velocity field of Sumatra and adjacent areas relative to the estimated Sunda Shelf reference frame. Ellipses indicate 2-D 95% confidence limits based on the formal (white noise only) uncertainty estimates, scaled by the goodness of fit of the Euler vector estimate (see Table 4). Shaded arrows show the principal strain rate axes for the northern, central, and southern parts of the Sumatra forearc (see also Table 5).

1996], extending roughly from the back arc of eastern Sumatra to eastern Borneo, southwestern Sulawesi (SW of the Palu fault), and Bali. There is some discussion as to what extent Southeast Asia, and consequently, the Sunda Shelf, behaves as a rigid plate and how much it is moving with respect to Eurasia. *Avouac and Tapponier* [1993], for example, fit a block model to shortening rates and slip rates (mostly derived from SPOT images) and deduce that South China moves SE relative to Siberia at a minimum rate of 10–15 mm/yr. In contrast, *England and Molnar* [1997] suggest (based on Quaternary fault slip rates) that lateral transport of Southeast Asian lithosphere is relatively minor, and that South China is moving ESE less than 10 mm/yr.

The GEODYSSSEA group has reported Sundaland motion relative to Eurasia of up to 12 mm/yr [*Chamot-Rooke and Le Pichon*, 1999; *Simons et al.*, 1999; *Michel et al.*, 2001].

[21] Our analysis shows that stations in South China and the Sunda Shelf are all moving significantly relative to Eurasia (Figure 3), but there is a large disparity between the uncertainties of the South China stations and some of the Sunda Shelf stations (Table 2). Stations BANJ, DENP, JOGY, KALP, KAYA, PANG, SUR, and TARA have uncertainties of up to 12 mm/yr in the east component and 3 mm/yr in the north because they were surveyed only twice (in 1992 and 1994). The mean velocity of these stations with respect to Eurasia: 7.1 ± 13.9 mm/yr east

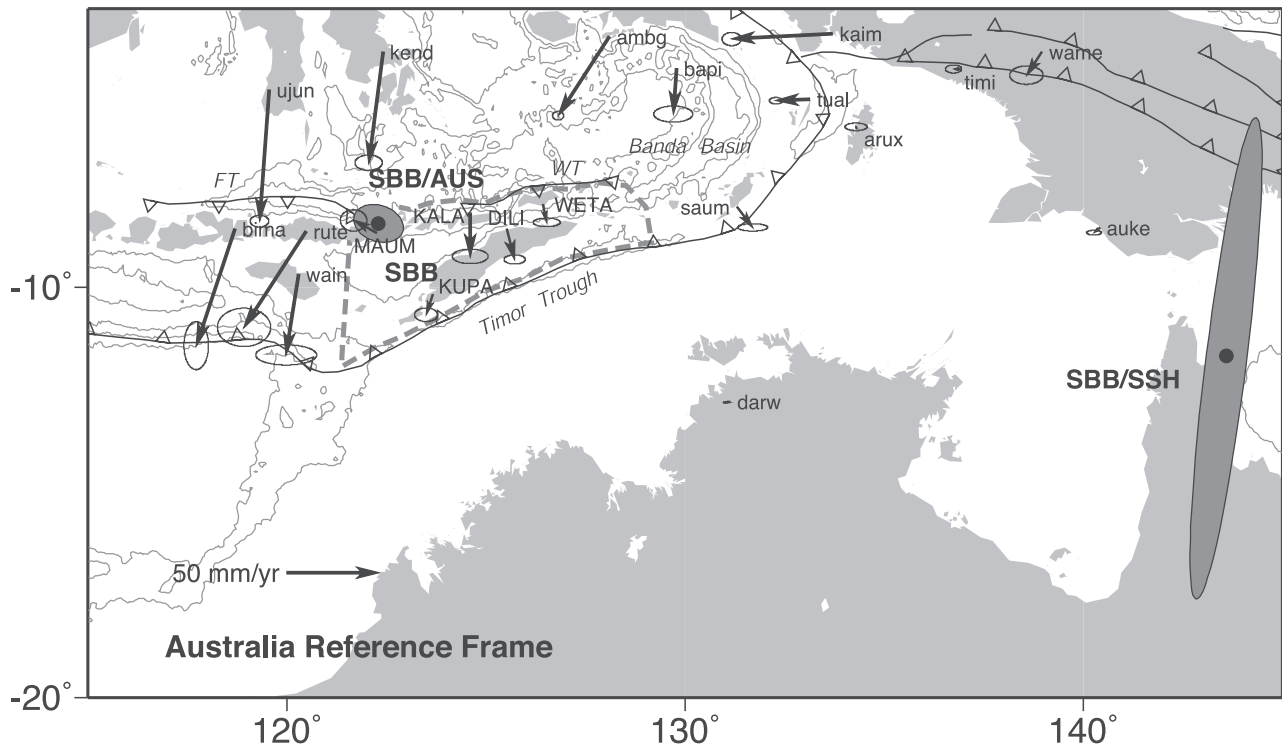


Figure 7. Velocity field of the SBB in the Australia reference frame. The five sites used to estimate the Euler pole for the SBB are labeled in capital letters (see also Table 2). Site velocity ellipses indicate 2-D 95% confidence limits based on the formal (white noise only) uncertainty estimates, scaled by the goodness of fit of the Euler vector estimate (see Table 4). Large dots with 1σ error ellipses indicate rotation poles of the SBB relative to the Australia and Sunda Shelf plates (see also Table 4). Heavy dashed lines indicate crustal block boundaries.

and 5.9 ± 6.8 mm/yr south. In contrast, the continuously tracking South China stations (XIAN, WUHN, SHAO, and TAIW) have velocity uncertainties of about 1.0 mm/yr or less. Stations BAKO, DEMU, and NTUS on the Sunda Shelf have similar uncertainties because the measurements span at least 4 years. Calculating the mean velocity at these seven sites, we conclude that there is 4.6 ± 2.4 mm/yr east and 3.6 ± 1.4 mm/yr south of Sunda Shelf motion relative to Eurasia.

[22] We next compute rotation parameters for the Sunda Shelf block (SSH) by minimizing the velocities of 16 stations in Indonesia and south China (Table 2 and Figure 4). Station KUNM was not included because of its proximity to the Red River and Xianshuihe faults and because its velocity is quite different from the 16 chosen Sunda Shelf stations. The 16 stations have a mean residual speed of 6.0 ± 13.7 mm/yr. The largest residuals occur at sites with the largest velocity uncertainties (Figure 4 and Table 2), suggesting that these residuals reflect the GPS velocity errors rather than nonrigid plate processes [Sella *et al.*, 2002].

[23] Our results indicate that the Sunda Shelf may be regarded as a distinct crustal block which extends to South China, and is moving at a rate of 6 ± 3 mm/yr in a roughly SE direction relative to Eurasia. This rate is lower than the 12 ± 3 mm/yr eastward motion reported by the GEODYSSSEA group for Sundaland (Indochina and western Indonesia) relative to Eurasia [e.g., Michel *et al.*, 2001]. Since our results include three sites with very precise velocities and a

much longer timespan (BAKO, DEMU, and NTUS), we suggest that our estimate is more reliable.

5.2. Sumatra

[24] Partitioning of oblique convergence along the plate boundary near Sumatra results in the formation of a forearc sliver block located between the Sumatran fault and Java trench (Figure 5). A previous study showed that azimuths of GPS velocities at sites on the southern part of the forearc (Siberut, Pagai, Enggano) are rotated clockwise relative to the forearc vectors on Nias and smaller islands further northwest, suggesting that the southern segment of the Sumatra subduction zone is currently locked, while the northern segment is less so [Prawirodirdjo *et al.*, 1997]. Our current results include an additional resurvey performed in 2001 of 26 sites on the Mentawai islands and the Sumatran coast, and are plotted in Figure 5 with respect to the Sunda Shelf. With the addition of data from the 2001 survey, the Sumatra forearc segmentation is still evident, although not as pronounced as before (Figure 5).

[25] Strain rates computed from GPS velocities of the forearc island and coastal sites indicate that the Sumatra forearc is experiencing significant arc-normal contraction (Table 5). There is also a small SE to NW increase in extension rates in the forearc (Table 5) suggesting a slight northward increase in slip rate along the Sumatran Fault [McCaffrey, 1991a]. Sieh *et al.* [1991, 1994] confirmed, from examining stream offsets in late Quaternary volcanic

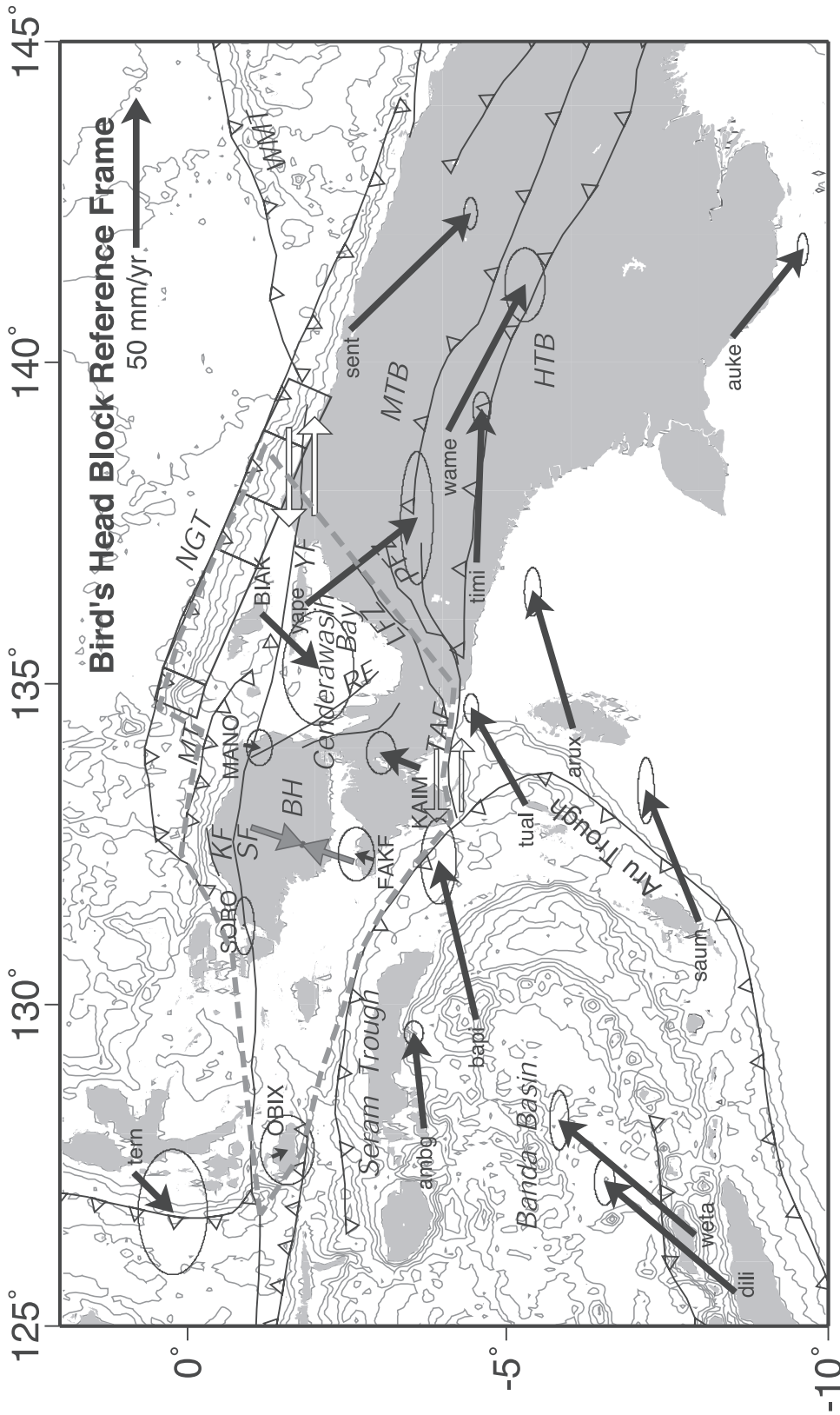


Figure 8. Velocity field derived from GPS surveys, in BHB reference frame, estimated by minimizing velocities at six sites (labeled in capital letters, see also Table 2), and after removing the modeled effect of strain accumulation at the NGT. Ellipses indicate 2-D 95% confidence limits based on the formal (white noise only) uncertainty estimates, scaled by the goodness of fit of the Euler pole estimate (see Table 4). Heavy lines show the modeled fault surface of the NGT. BH, Bird's Head; HTB, Highlands thrust belt; KF, Koor fault; LFZ, Lowlands fault zone; MT, Manokwari trench; MTB, Mamberamo thrust belt; NGT, New Guinea trench; PFZ, Paniai fault zone; RF, Ransiki fault; SF, Sorong fault; TAF, Tarara-Aiduma fault; WMT, West Melanesia trench; YF, Yapen fault. Open arrows show sense of slip along Yapen and Tarara-Aiduma Faults. Shaded strain axis shows internal strain rate for the BHB. Values for the strain rates are given in Table 5. Heavy dashed lines indicate crustal block boundaries.

Table 4. Block Angular Velocities^a

Block Pair	Reference	Latitude, °N	Longitude, °E	ω , deg/Myr	Pole Error Ellipse			χ^2
					σ_{maj}	σ_{min}	Azim.	
EUR-NNR	<i>Larson et al.</i> [1997]	56.3	-102.8	0.26 ± 0.02	5.7	1.7	43	...
EUR-ITRF1997	<i>Sella et al.</i> [2002]	58.27	-102.21	0.257 ± 0.003	1.5	0.4	34	1.02
EUR-ITRF2000	this study	58.3	-97.2	0.26 ± 0.00	1.5	0.3	48	1.8
SSH-ITRF2000	this study	49.4	-95.9	0.32 ± 0.01	3.5	1.0	121	1.2
AUS-NNR	<i>Larson et al.</i> [1997]	31.4	40.7	0.61 ± 0.01	3.1	1.0	-61	...
AUS-ITRF2000	<i>Tregoning</i> [2002]	35.1	36.5	0.619 ± 0.004	0.8	0.3	287	...
AUS-ITRF2000	<i>Beavan et al.</i> [2002]	32.76	37.54	0.621 ± 0.002	0.4	0.13	109	1.08
AUS-ITRF1997	<i>Sella et al.</i> [2002]	34.86	38.26	0.627 ± 0.004	1.2	0.4	-65	2.78
AUS-ITRF2000	this study	33.0	38.1	0.62 ± 0.00	1.0	0.2	152	1.2
PAC-NNR	<i>Larson et al.</i> [1997]	-63.1	95.9	0.70 ± 0.01	2.3	0.9	-82	...
PAC-ITRF2000	<i>Tregoning</i> [2002]	-64.3	114.2	0.649 ± 0.005	1.6	0.4	82	...
PAC-ITRF2000	<i>Beavan et al.</i> [2002]	-63.75	110.86	0.68 ± 0.00	0.61	0.15	85	0.93
PAC-ITRF1997	<i>Sella et al.</i> [2002]	-64.21	112.74	0.655 ± 0.004	0.7	0.4	75	1.2
PAC-ITRF2000	this study	-65.0	110.3	0.67 ± 0.01	1.8	0.5	9	0.9
SBB-ITRF2000	this study	17.5	-43.0	2.11 ± 0.74	7.5	0.8	34	2.0
SBB-AUS ^b	this study	-8.4	122.3	-2.50 ± 0.26	0.3	0.1	109	7.4
SBB-SSH ^b	this study	-11.7	143.6	-1.76 ± 0.39	6.1	0.5	7	7.7
BHB-ITRF2000	this study	-6.4	127.0	3.55 ± 0.45	1.4	0.4	36	2.2
BHB-AUS ^b	this study	-14.2	136.6	2.92 ± 0.45	2.92	0.5	107	2.3

^aPlate velocities are given as rotation of the first-named plate relative to the second. The ω is positive for anticlockwise rotation. The σ_{maj} and σ_{min} are the major and minor axes of the pole error ellipse, with the azimuth of the major axis given CCW from east. NNR refers to the no-net-rotation NUVEL-1A reference frame. The χ^2 values, given for estimates performed in this study, refer to the sum of squared weighted residuals, normalized by the degrees of freedom. N is the number of stations used to estimate block rotation parameters. AUS, Australia plate; BHB, Bird's Head Block; EUR, Eurasia plate; SBB, South Banda Block; SSH, Sunda Shelf Block.

^bThese poles were computed by combining poles, which were derived relative to ITRF2000.

tuff, a NW increase in the geologic slip rate: from about 11 mm/yr between 0° and 3.5°S, to 28 mm/yr near 2.2°N. *Sieh and Natawidjaja* [2000] suggest that a belt of auxiliary, transtensional deformation in the forearc sliver is the nascent manifestation of this rate change.

[26] The velocity estimates for sites in southern Sumatra are not well constrained (Figure 5) and cannot be used to perform a detailed analysis of deformation in the southern Sumatran fault and forearc. Nevertheless, the north components of sites JAMB and KALP suggest that the southern part of the back arc moves similarly to the northern part. If we assume that the entire Sumatra back arc is not deforming significantly, then the arc-parallel components of KULU and ENGG suggest that the southern part of Sumatran Fault slips at a lower rate than the northern part (Figure 5). This observation would be consistent with the prediction of a northward increase in slip rates on the fault based on subduction earthquake slip vectors [*McCaffrey*, 1991a], and with geological slip rate estimates (e.g., 11 mm/yr

between 0° and 3.5°S [*Sieh et al.*, 1994], 5.5 ± 1.9 mm/yr at 5°S [*Bellier et al.*, 1999]).

5.3. Eastern Boundary of the Sunda Shelf

[27] On its eastern boundary, the SSH converges with the Philippine Sea and Pacific plates. Velocities at MANA, (NE Sulawesi), and the two Moluccan sites, TERN and OBIX, show the rapid east-west convergence between the Pacific plate and Southeast Asia. Motion of TERN relative to MANA (Figure 4) indicates 84.8 ± 10.0 mm/yr of east-west shortening across the Molucca Sea collision zone [*McCaffrey*, 1991b]. At the latitude of OBIX, the convergence of the Sunda Shelf with the Pacific plate is buffered by the East Sulawesi block, resulting in rapid clockwise rotation of the East Sulawesi block (MANA and LUWU, Figure 4) relative to the Sunda Shelf [*Stevens et al.*, 1999]. This block rotation transfers about one third of the Pacific-Sunda Shelf convergence to left-lateral slip along the Palu fault and north-south shortening across the North Sulawesi

Table 5. Internal Strain Rates of Regional Tectonic Blocks in Indonesia^a

Region	ϵ_{11} , 10^{-6}	Azimuth of ϵ_{11}	ϵ_{22} , 10^{-6}	CW Rotation Rate, 10^{-6} Per Year	χ^2	N
	Per Year		Per Year			
Sunda Shelf Block	-0.001 ± 0.000	22.5 ± 6.3	0.003 ± 0.001	0.003 ± 0.0001	2.1	16
South Banda Block	0.005 ± 0.018	26.3 ± 17.6	0.045 ± 0.017	0.001 ± 0.016	9.4	5
Bird's Head Block	-0.064 ± 0.010	20.1 ± 7.1	-0.003 ± 0.009	-0.055 ± 0.008	3.1	6
North Sumatra Forearc (D952,D953,D962,BINT, JULU,PAND,SIKA)	-0.081 ± 0.017	34.2 ± 6.4	0.012 ± 0.016	0.0441 ± 0.012	0.8	8
Central Sumatra Forearc (D944,D947,D949,AIRB,AJUN,NSIB,SIKA,TOBO)	-0.080 ± 0.012	29.9 ± 5.0	0.016 ± 0.011	0.004 ± 0.008	2.1	7
South Sumatra Forearc (D937,P003,PADA, PAGA,SIOB)	-0.097 ± 0.014	30.5 ± 10.1	-0.026 ± 0.017	1.989 ± 14.833	1.4	5

^aThe x axis points eastward, the y axis points northward, and are the principal strain rate axes of maximum compression and extension, respectively. N is the number of GPS vectors used in the strain estimation. The χ^2 is the sum of the residuals squared divided by their individual standard deviations squared, then divided by the degrees of freedom ($2N - 6$).

trench as the Celebes Sea subducts beneath it (Figure 4). It has been suggested that block rotations about a nearby vertical axis are an efficient mechanism for shortening in continents [McKenzie and Jackson, 1983]. In this case the process is further facilitated by the presence of oceanic lithosphere north of Sulawesi, providing a way for continental collision to be at least partly accommodated by subduction of gravitationally unstable oceanic crust. Consequently, not far south of TERN and MANA, the east-west shortening rate between OBIX and LUWU is only 37.2 ± 5.3 mm/yr (Figure 4). From surveying a transect of GPS stations spanning the Palu fault, Stevens *et al.* [1999] estimate a slip rate of 38 ± 8 mm/yr, and a locking depth of 2–8 km. This slip rate is consistent with 40–50 mm/yr of convergence along the northern arm of Sulawesi deduced from geologic and paleomagnetic data [Walpersdorf *et al.*, 1998].

[28] On the island of Flores at 122°E , an abrupt change in the velocity field (Figure 4) occurs as the oceanic lithosphere subducting beneath the Java trench turns into the Australian continental shelf, and the Sunda Shelf continental lithosphere thins and transitions into oceanic crust [Curray *et al.*, 1977]. The associated deformation at the margin of the Sunda Shelf is accommodated by north-trending strike-slip faults in the upper plate, evidenced by focal mechanisms of shallow earthquakes just west of Sumba [McCaffrey, 1989]. Flores was also the location of a large ($M_w = 7.9$) thrust earthquake on 12 December 1992. The earthquake was a shallow back arc thrust event on the Flores thrust [Beckers and Lay, 1995]. Our measured velocity for MAUM, on Flores, relative to KEND (Figure 4) is 67 ± 4 mm/yr; however, this may be an overestimate of the shortening rate across the Flores Sea because our estimate includes measurements taken in December 1992, shortly after the earthquake, and thus probably contains a postseismic signal.

6. Motion Relative to Australia

6.1. Australia Pole of Rotation

[29] The Euler vector for Australia relative to ITRF2000 is computed by minimizing station velocities of stations on Australia, Tasmania, Cocos Island, Noumea, and Auckland (Figure 6). Formal velocity uncertainties for many sites on the Australia plate are significantly lower than for other sites, due to the long time span of observations (most of the stations have been operational since 1991). We found that using a weight of $(3\sigma)^{-2}$ in the Euler vector estimation for Australia gave a $\chi^2 \approx 1$ (Table 4). Our estimated rotation pole for Australia is consistent with the one estimated by Beavan *et al.* [2002] (Table 4). The mean residual speed for the Australia plate stations (Figure 6 and Table 2) is 1.8 ± 1.6 mm/yr. A few stations (Table 2) show residual velocities slightly higher than the upper bound of 2 mm/yr of the best observed intraplate sites [Argus and Gordon, 1996], but our results are still consistent with the finding of Tregoning [2002] that the Australia plate may be considered a rigid plate extending as far as Noumea, Auckland, and Cocos.

[30] Three Indonesian sites north of Australia (ARUX, AUKE, and TIMI) have insignificant velocities relative to Australia (Table 2), indicating that there is little or no deformation between northern Australia and southern New Guinea.

[31] Station SENT in northern New Guinea moves at a rate of 26.7 ± 1.5 mm/yr west and 18.5 ± 0.6 mm/yr south relative to Australia, confirming that only a fraction of the expected 95 mm/yr shear and 55 mm/yr shortening between the Pacific and Australia plates occurs on the island.

6.2. Convergence Across the Java Trench

[32] The oceanic part of the Australian plate (the Indian Ocean lithosphere) is subducting beneath the Java trench. The NUVEL-1A model predicts a convergence rate of 71 mm/yr in a $\text{N}20^\circ\text{E}$ direction at the longitude of 107°E at the Java trench. The average earthquake slip vector azimuth south of Java (between 105°E and 110°E) is $\text{N}11^\circ \pm 9^\circ\text{E}$ and repeated (1989–1993) GPS measurements of a single trench-crossing baseline indicated a convergence rate of 67 ± 7 mm/yr [Tregoning *et al.*, 1994]. Our extended time series allows us to update the estimate of convergence rate across the Java trench. Our observed GPS velocity for site BAKO relative to the Australia plate (Figure 6) is 63.3 ± 0.4 mm/yr at $\text{N}14.9^\circ \pm 0.5^\circ\text{E}$, slightly slower and less northerly than the less precise estimate of Tregoning *et al.* [1994].

6.3. Collision of Banda Arc With Australia

[33] The Banda arc is colliding with continental Australia to the south and with northwest New Guinea (Bird's Head) to the north (Figures 4 and 6). Genrich *et al.* [1996] showed that sites on the islands of Timor, Alor, Wetar, and East Flores defined a discrete SBB. Assuming that subduction occurred at the Timor trench in the past, the SBB has now largely accreted to the Australian plate. Our GPS velocity field shows that sites on the south Banda arc (DILI, KALA, KUPA, MAUM, SAUM, and WETA) are converging with Australia at a mean rate of 15.0 ± 7.7 mm/yr (Table 2 and Figure 6), a small fraction of the 70 mm/yr rate of Australia-Eurasia convergence. This confirms the result of Genrich *et al.* [1996] that convergence at this boundary zone is dominated by back arc thrusting.

[34] Although the inferred 15.0 ± 7.7 mm/yr rate across the Timor trough is quite low, it is still significant and does not rule out the possibility of a large earthquake at the Timor trough and the SW end of the Aru trough where SAUM is located. Further east along the Banda arc, velocities at TUAL and ARUX (Figures 6 and 7) indicate divergence instead of convergence. It is important to note that the collision trace passes just west of the island of Kai Besar, on which TUAL is located [Milsom *et al.*, 1996], thus both TUAL and ARUX are located east of the thrust boundary, and the apparent 18 mm/yr divergence between ARUX and TUAL is occurring within the Australia plate.

[35] We estimate an Euler vector for the SBB using sites WETA, DILI, KALA, KUPA, and MAUM, excluding SAUM because its velocity is significantly different from the other sites. The poor fit for the estimated SBB pole (Table 4) reflects the block's significant internal deformation. The SBB rotates rapidly about a nearby axis relative to the larger Sunda Shelf and Australia blocks (Figure 7). We also estimate the rotation poles for the SBB relative to the Sunda Shelf and Australia (Figure 7 and Table 4). The two poles are located within the region near the SBB. Estimation of an average strain rate for the SBB suggests that internally, the SBB is dominated by arc-normal extension, although the

poor fit for the strain rate estimate (Table 5) indicates that the strain is not uniform.

[36] The deformation increases west of the SBB, along the Banda arc region from Sumba to Flores. This velocity transition coincides with the transition of continental crust into oceanic crust north of the island arc. Sites just west of the SBB move roughly SSW relative to the SBB (Figure 7), and this SW trending motion increases rapidly westward in magnitude. *McCaffrey* [1988] proposed, based on a study of shallow earthquake focal mechanisms, that this part of the South Banda arc is segmented by several NNE trending, left-lateral strike-slip faults. The GPS vectors here are consistent with this theory. BIMA and RUTE are moving left-laterally relative to KALA, KUPA, and WAIN. The region of the Banda forearc, from Sumbawa to the Sumba and Sawu basins (the region spanned by BIMA, RUTE, and WAIN), is a small, rapidly deforming segment of the forearc lying between the Sunda Shelf and SBBs. It represents the transition between subduction at the Java trench to the west and back arc thrusting north of Flores and Timor.

[37] At the eastern part of the Banda arc, the Banda basin is spanned by the SBB stations in the south and stations AMBG and BAPI in the north (Figure 7). Fault plane solutions of shallow earthquakes in the Banda basin suggest that it contracts north-south and extends east-west by a combination of strike-slip and thrust faulting [*McCaffrey*, 1988]. Motion at AMBG, which was observed over a span of 8 years, is much better constrained than motion at BAPI. Site AMBG (Figure 7) moves 46.4 ± 1.1 mm/yr west and 20.0 ± 0.9 mm/yr south with respect to the SBB, representing roughly the rates of strike-slip and thrust faulting, respectively, within the Banda Sea. The east-west extension within the Banda basin is also reflected in the relative motion between AMBG and BAPI (Figure 7).

7. Motion Relative to the Pacific Plate

7.1. Pacific Plate Pole of Rotation

[38] For the Pacific plate, only five station velocities (Figure 1) were available to us for computing rotation parameters. Nevertheless, our computed pole for the Pacific plate is consistent with the latest Pacific pole computed by *Beavan et al.* [2002] from 12 station velocities. The New Guinea Trench (NGT) was the site of the $M_w = 8.2$ Biak earthquake in 1996 [*Masturyono et al.*, 1998]. Velocities for BIAK, MANO, and YAPE do not include measurements made in 1996 after this earthquake and reflect locking at the NGT during the period before the earthquake [*Okal*, 1999].

7.2. Bird's Head Block

[39] The Bird's Head portion of New Guinea is separated from the rest of New Guinea by the TAF and the Highlands thrust belt. Additional faults may be active in the vicinity of Bird's Neck (the Wandamen fault zone, Lengguru fold belt, and Arguni fault [*Dow and Sukamto*, 1984]), while the Bird's Head itself is the location of the Sorong, Koor, and Ransiki faults (Figure 8).

[40] Rotation of the BHB relative to the Australia plate was estimated from measurements at sites BIAK, MANO, KAIM, FAKF, SORO, and OBIX (Table 2). These sites are

located near the NGT, which was locked during the period before the 1996 Biak earthquake [*Okal*, 1999]. Before estimating rotation parameters for this block, we remove the effect of strain accumulation on the NGT. We model the locked portion of the NGT as a ~ 600 -km-long fault dipping 11° to the SW, and extending from the surface down to 15 km depth (Figure 8). The fault dip and depth extent are based on the Harvard CMT focal mechanism for the 1996 Biak earthquake. The fault length is based on geological estimates of the active portion of the NGT [*Okal*, 1999]. In effect, we subtract an inferred SW component out of the GPS-derived velocities for stations BIAK, YAPE, and MANO due to the southwestward subduction at the NGT.

[41] Our estimated rotation parameters show the BHB moving rapidly WSW relative to Australia (Figure 6), subducting underneath the Seram trough (northern Banda arc) in the process. The southwestward direction of subduction is consistent with focal mechanisms of relocated deep earthquakes in the Banda Basin (e.g., most recently, H. Schöffel and S. Das, personal communication). Principal strain axes estimated from velocities at sites on the BHB (Table 5) reveal the deformation to be dominated by compression consistent with the direction of convergence across the NGT.

7.3. Sorong, Yapen, and Tarera-Aiduna Faults

[42] The velocity field shown in Figure 8 suggests some left-lateral motion of SORO relative to FAKF and KAIM. This velocity gradient could be due to strain accumulation along the Sorong or Koor faults. (Relocation of historical seismicity by *Okal* [1999] in the BHB region is more consistent with slip on the Koor fault than on the Sorong fault.) At 128°E longitude, left-lateral motion of Ternate (TERN) relative to the BHB (Figure 8) suggests 19 ± 8 mm/yr slip along the westward continuation of the Sorong fault.

[43] The eastward continuation of the Sorong fault, also known as the Yapen fault, appears to be slipping at a high rate, as seen in 46 ± 12 mm/yr of left-lateral motion between MANO-BIAK and YAPE-SENT (Figure 8). The Sorong fault system from the Mamberamo belt to Cenderawasih Bay is seismically active [*Okal*, 1999]. GPS measurements also show 21 ± 9 mm/yr of left-lateral motion between YAPE-SENT and TIMI-WAME, indicating that some of the left-lateral convergence component may be accommodated within the Highlands thrust belt. This is consistent with strike-slip focal mechanisms identified by *Abers and McCaffrey* [1988] within the mountain belt.

[44] To the south, motion of TIMI relative to Bird's Head (Figure 8) implies high slip rates on the TAF. *Seno and Kaplan* [1988] identified two $M_s > 6$ shallow earthquakes in the locality of the TAF, with strike-slip focal mechanisms that are consistent with left-lateral slip along the TAF.

[45] At the longitude of 134°E , most of the BHB motion relative to Australia occurs south of Bird's Head, near the TAF, while at 137°E , the motion occurs more to the North, near the Yapen fault (Figure 8). The transfer of slip between these two fault zones would lead us to infer the existence of active extensional structures in the Bird's Neck region or in Cenderawasih Bay. Geological mapping,

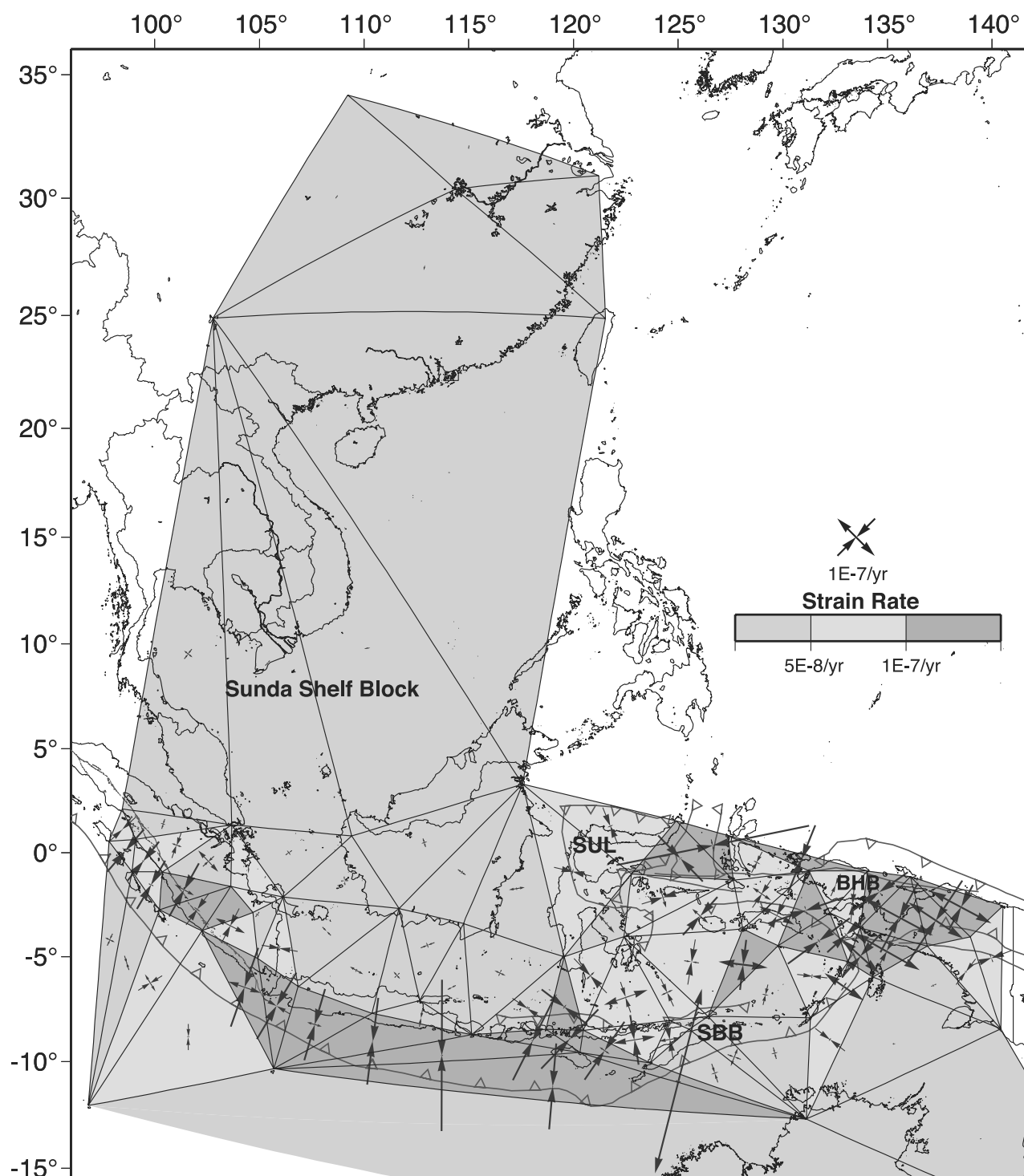


Figure 9. Principal surface strain rates (dark blue arrows indicating contraction/extension) computed for triangular elements (boundaries indicated by solid lines) with nodes located at GPS stations. Elements are shaded light green for corresponding strain rates smaller than 5×10^{-8} per year, yellow for rates between 5×10^{-8} and 10^{-7} per year, and mustard colored for rates exceeding 10^{-7} per year. Red lines trace faults. SUL, East Sulawesi Block; BHB, Bird's Head Block; SBB, South Banda Block. See color version of this figure at back of this issue.

however, shows structures in the Bird's Neck region, which are predominantly compressional and strike slip [Dow and Sukanto, 1984]. A more likely scenario, proposed by Stevens *et al.* [2002] is that shear between the BHB and

Australia is distributed along the NE trending lowlands and Paniai fault zones (Figure 8) which truncate the western end of the main Highlands Thrust Belt, and that the apparent extension in the Bird's Neck region (Figure 8)

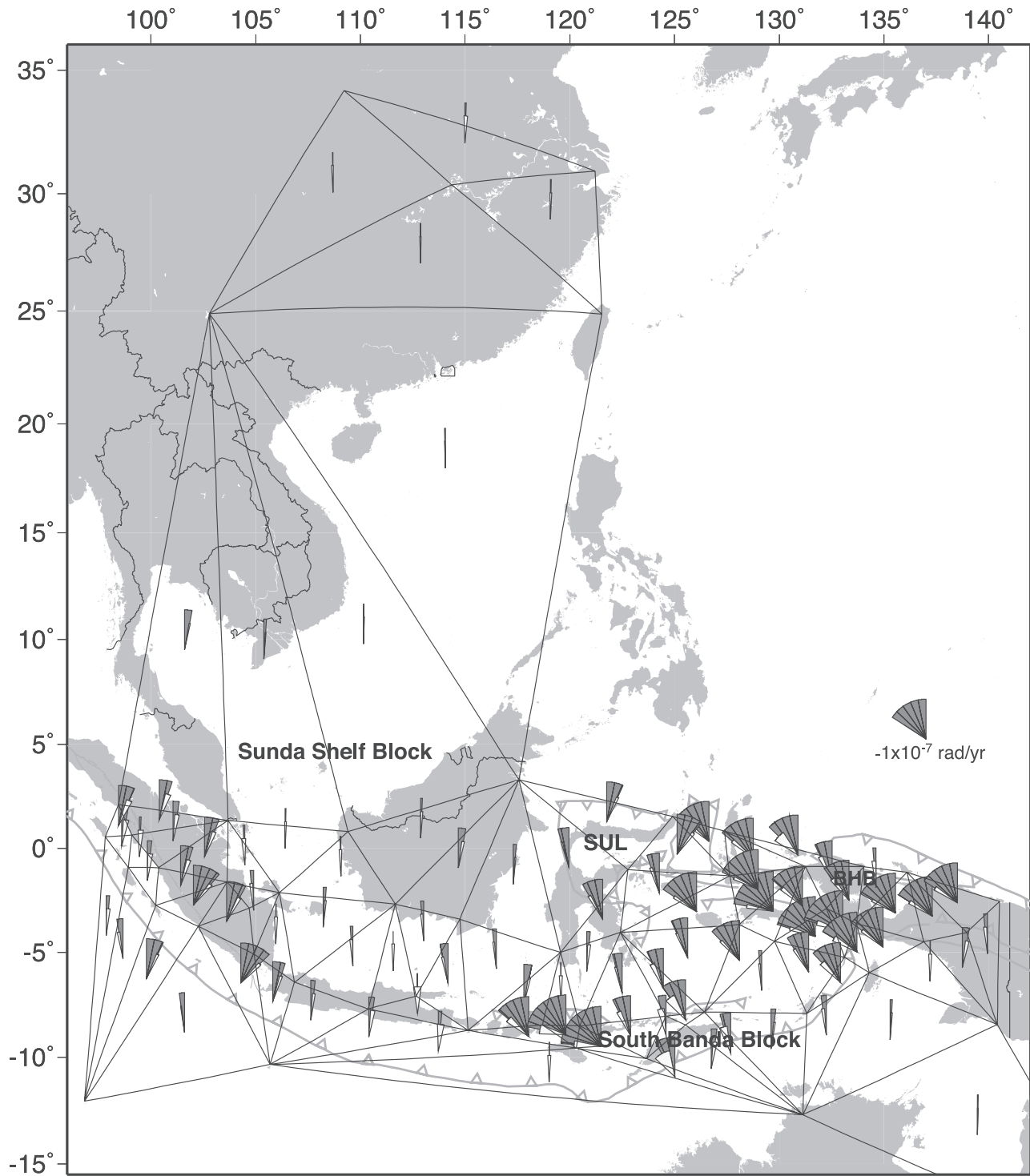


Figure 10. Rotation rates computed for triangular elements (boundaries indicated by solid lines) with nodes located at GPS stations. The rate is proportional to the angle spanned by the dark shaded rotation wedge (scale is given in upper right corner). Light shaded wedges indicate rotation uncertainties. SUL, East Sulawesi Block, BHB, Bird's Head Block.

can be explained by the presence of rotating crustal blocks within the shear zone.

8. Strain Rates

[46] We have described the regional kinematics in terms of distinct crustal blocks rotating relative to one another in a

manner analogous to global-scale plate tectonics [Thatcher, 1995]. To further explore the potential application of this concept to Indonesian neotectonics, we examine the regional strain rates in more detail using our observed GPS-derived velocities.

[47] We compute strain rates within elements of a triangular mesh with nodes at our GPS stations (Figure 9).

Rotation rates of the triangle elements are shown in Figure 10. For clarity, we do not use all our GPS vectors in Sumatra, selecting instead only three forearc island sites, three coastal sites, and four back arc sites to represent the strain rates in and around Sumatra.

[48] The Sunda Shelf and SBBs have strain rates consistently lower than $5 \times 10^{-8} \text{ yr}^{-1}$. Mesh elements spanning the Timor trough also have strain rates of $\sim 10^{-8}$ per year. In contrast, elements spanning the Molucca Sea, Seram trough, TAF, and the Sumatra-Java trench have strain rates exceeding 10^{-7} per year. Strain rates of triangles located on the East Sulawesi and BHBs fall between 5×10^{-8} and 10^{-7} per year, similar to strain rates in the western Banda basin and at the Sumatran fault (Figure 9).

[49] Deformation in eastern Indonesia is clearly more distributed and complex than in the west. In western Indonesia, deformation is limited to the Sumatran fault and the Sumatra-Java trench and is comparatively simple, dominated largely by trench-normal contraction. In contrast, deformation in eastern Indonesia varies and includes significant anticlockwise rotations (Figure 10). Large ($>10^{-7}$ rad/yr) anticlockwise rotations are especially evident in mesh elements spanning the Sumba forearc, the northern Banda arc, and the Bird's Head region (Figure 10).

[50] Internal strain rates for the SSH are an order of magnitude lower than those for the deformation zone separating it from the Australia plate. Furthermore, the SSH lacks any known active faults in its interior and is much larger than the deformation zone bordering it to the south. The SSH thus fits the description of *Thatcher* [1995] of a continental microplate. The smaller South Banda, East Sulawesi, and BHBs are deforming at significantly higher rates and are part of the wide deformation zone that covers much of eastern Indonesia.

9. Summary and Conclusions

[51] We present a regional velocity field derived from GPS data obtained in the Indonesian archipelago over the past 10 years. This field forms a critical basis for testing models of current plate kinematics and plate boundary deformation in Southeast Asia. The observed velocities confirm four large-scale tectonic regimes: frontal subduction south of Java, oblique subduction offshore of Sumatra, frontal collision between Australia and southeastern Indonesia, and oblique collision between the Pacific and Australia in western New Guinea. Within the broad plate boundary region, we identify four distinct crustal blocks: the Sunda Shelf, East Sulawesi, South Banda, and Bird's Head Blocks.

[52] The SSH includes much of Indochina and is moving 6 ± 3 mm/yr SE relative to the Eurasia plate. The southern part of New Guinea is stationary relative to Australia.

[53] The South Banda block rotates clockwise relative to both the Sunda Shelf and Australia, resulting in 15 ± 8 mm/yr of motion across the Timor trough, 59 ± 3 mm/yr of shortening across the Flores Sea, and up to 50 mm/yr shortening across the Banda Sea.

[54] The East Sulawesi block rotates clockwise around a pole located near NE Sulawesi, transferring east-west con-

vergence into north-south shortening north of Sulawesi and left-lateral slip on the Palu fault.

[55] In the case of the South Banda and East Sulawesi blocks, placement of relatively small pieces of oceanic and continental crust appears to dictate the regional kinematics. In this collisional setting, the active processes seek the path of least resistance, which is subduction of oceanic crust beneath continental crust [Molnar and Gray, 1979], and results in the aforementioned block rotations.

[56] The BHB is moving rapidly WSW relative to Australia and southeastern New Guinea. The resulting left-lateral shear zone may be as wide as 300 km [Stevens *et al.*, 2002], composed of several strike-slip faults, and accommodates up to 80 mm/yr of left-lateral strike slip. Sites of rapid convergence (>50 mm/yr) include the Java trench, Molucca Sea, and Seram trough. Lower rates (<40 mm/yr) of convergence probably occur at the North Sulawesi, New Guinea, and Manokwari trenches.

[57] Active tectonics in Indonesia exhibits kinematic motions which are well described in terms of discrete tectonic blocks rotating relative to one another. However, except for the Sunda Shelf, the crustal blocks do not fit the microplate tectonics model in the sense that they are experiencing significant internal deformation.

[58] **Acknowledgments.** This work is part of a collaborative agreement between the Indonesian National Coordination Agency for Surveying and Mapping (BAKOSURTANAL), Rensselaer Polytechnic Institute, and Scripps Institution of Oceanography. We are indebted to Jakob Rais for his encouragement and support of our work in Indonesia since its inception, and to the BAKOSURTANAL management including Joenil Kahar, Rudolph Matindas, Klass Villanueva, and the late Paul Suharto. Site monumentation and data collection for this study could only have been accomplished with the help of many Indonesian and U.S. surveyors, in particular, Chris Bagandi, Heru Derajat, Djawahir, Endang, Nyamadi, Ponimin, Rustandi Poewariardi, Untung Santoso, Bambang Susilo, Widiyanto, and Didi Wikayardi from Indonesia, and Dan Johnson, Dalia Lahav, Brennan O'Neill, Craig Roberts, Jennifer Scott, Mara Yale, and Peter Zwick from U.S. institutions. We are grateful to James Stowell and his staff (Bruce Stephens and Mike Jackson) at the UNAVCO Boulder facility for training and providing field engineers for the early Sumatra surveys. Joe Bearden from Caltex provided logistical support and GPS receivers for surveys in eastern Sumatra. We thank Paul Tregoning and Shimon Wdowinski for their input to the data analysis. Australian tracking data were organized and provided by Ken Alexander, Fritz Brunner, Martin Hendy, John Manning, and Paul Tregoning. Fugro Survey provided Denpasar data in 1993. Miranda Chin and Gerry Mader provided CIGNET data. We thank Peng Fang and Rosanne Nikolaidis of the Scripps Orbit and Permanent Array Center for supplying precise satellite ephemerides and global GPS solutions, and colleagues from the International GPS Service for global tracking data since 1992. Figures were drawn with GMT [Wessel and Smith, 1991]. Supported at SIO by NSF grants EAR-8817067, EAR-9004376, EAR00-01090, and NASA grant NAGW-2641, at RPI by NSF grants EAR-8908759 and EAR-9114349, and by the Indonesian government.

References

- Abers, G., and R. McCaffrey, Active deformation in the New Guinea fold-and-thrust belt: Seismological evidence for strike-slip faulting and basement-involved thrusting, *J. Geophys. Res.*, *93*, 13,332–13,354, 1988.
- Argus, D. F., and R. G. Gordon, Tests of the rigid-plate hypothesis and bounds on intraplate deformation using geodetic data from very long baseline interferometry, *J. Geophys. Res.*, *101*, 13,555–13,572, 1996.
- Avouac, J. P., and P. Tapponier, Kinematic model of active deformation in central Asia, *Geophys. Res. Lett.*, *20*, 895–898, 1993.
- Barber, A. J., and M. J. Audley-Charles, The significance of metamorphic rocks of Timor in the development of the Banda arc, eastern Indonesia, *Tectonophysics*, *30*, 119–128, 1976.

- Beavan, J., P. Tregoning, M. Bevis, T. Kato, and C. Meertens, Motion and rigidity of the Pacific plate and implications for plate boundary deformation, *J. Geophys. Res.*, 107(B10), 2261, doi:10.1029/2001JB000282, 2002.
- Beckers, J., and T. Lay, Very broadband seismic analysis of the 1992 Flores, Indonesia, earthquake, ($M_w = 7.9$), *J. Geophys. Res.*, 100, 18,179–18,193, 1995.
- Bellier, O., H. Bellon, M. Sébrier, and R. C. Maury, K-Ar age of the Ranau Tuffs, implications for the Ranau caldera emplacement and slip-partitioning in Sumatra (Indonesia), *Tectonophysics*, 312, 347–359, 1999.
- Bock, Y., et al., Southern California permanent GPS geodetic array: Continuous measurements of crustal deformation between the 1992 Landers and 1994 Northridge earthquakes, *J. Geophys. Res.*, 102, 18,013–18,033, 1997.
- Bock, Y., R. Nikolaidis, P. Fang, and M. Van Domselaar, Re-analysis of a decade of continuous GPS data at the Scripps Orbit and Permanent Array Center: Implications for terrestrial reference frame stability, *Eos Trans. AGU*, 82(47), Fall Meet. Suppl., Abstract F278, 2001.
- Cardwell, R. K., and B. L. Isacks, Geometry of the subducted lithosphere beneath the Banda Sea in eastern Indonesia from seismicity and fault plane solutions, *J. Geophys. Res.*, 83, 2825–2838, 1978.
- Chamot-Rooke, N., and X. Le Pichon, GPS determined eastward Sundaland motion with respect to Eurasia confirmed by earthquake slip vectors at Sunda and Philippine trenches, *Earth Planet. Sci. Lett.*, 173, 439–455, 1999.
- Curry, J. R., G. G. Shor Jr., R. W. Raitt, and M. Henry, Seismic refraction and reflection studies of crustal structure of the eastern Sunda and western Banda arcs, *J. Geophys. Res.*, 82, 2479–2489, 1977.
- DeMets, C., R. Gordon, D. Argus, and S. Stein, Effects of recent revisions to the geomagnetic reversal time scale on estimates of current plate motions, *Geophys. Res. Lett.*, 21, 2191–2194, 1994.
- Dow, D. B., and R. Sukanto, Western Irian Jaya: The end-product of oblique plate convergence in the Tertiary, *Tectonophysics*, 106, 109–139, 1984.
- England, P., and P. Molnar, The field of crustal velocity in Asia calculated from Quaternary rates of slip on faults, *Geophys. J. Int.*, 130, 551–582, 1997.
- Fitch, T. J., Plate convergence, transcurrent faults and internal deformation adjacent to Southeast Asia and the western Pacific, *J. Geophys. Res.*, 77, 4432–4460, 1972.
- Genrich, J. F., Y. Bock, R. McCaffrey, E. Calais, C. W. Stevens, and C. Subarya, Accretion of the southern Banda arc to the Australian plate margin determined by Global Positioning System measurements, *Tectonics*, 15, 288–295, 1996.
- Genrich, J. F., Y. Bock, R. McCaffrey, L. Prawirodirdjo, C. W. Stevens, S. S. O. Puntodewo, C. Subarya, and S. Wdowski, Distribution of slip at the northern Sumatran fault system, *J. Geophys. Res.*, 105, 28,327–28,341, 2000.
- Hamilton, W., Tectonics of the Indonesian region, *U.S. Geol. Surv. Prof. Pap.* 1078, U. S. Geol. Surv., Boulder, Colo., 1979.
- Herring, T., *Global Kalman Filter VLBI and GPS Analysis Program (GLOBK)*, version 5.0, Mass. Inst. of Technol., Cambridge, Mass., 2000.
- Jacobson, R. S., G. G. Shor Jr., R. M. Kieckhefer, and G. M. Purdy, Seismic refraction and reflection studies in the Timor-Aru trough system and Australian continental shelf, in *Geological and Geophysical Investigations of Continental Margins*, edited by J. S. Watkins, *Am. Assoc. Pet. Geol. Mem.*, 29, pp. 209–222, Am. Assoc. of Pet. Geol., Tulsa, Okla., 1979.
- King, R., and Y. Bock, *Documentation for the GAMIT GPS Analysis Software, Release 9.94*, Mass. Inst. of Technol., Cambridge, Mass. and Scripps Inst. of Oceanogr., La Jolla, Calif., 2000.
- Larson, K. M., and D. C. Agnew, Application of the Global Positioning System to crustal deformation measurement: 1. Precision and accuracy, *J. Geophys. Res.*, 96, 16,547–16,565, 1991.
- Larson, K. M., J. T. Freymueller, and S. Philipsen, Global plate velocities from the global positioning system, *J. Geophys. Res.*, 102, 9961–9981, 1997.
- Masturyono, F., et al., Rupture zone of the Biak earthquake of February 17, 1998 inferred from aftershocks, coseismic deformation, and waveform analysis, *Eos Trans. AGU*, 79(45), Fall Meet. Suppl., F573, 1998.
- McCaffrey, R., Active tectonics of the eastern Sunda and Banda arcs, *J. Geophys. Res.*, 93, 15,163–15,182, 1988.
- McCaffrey, R., Seismological constraints and speculation on Banda arc tectonics, *Neth. J. Sea Res.*, 24, 141–152, 1989.
- McCaffrey, R., Slip vectors and stretching of the Sumatra fore arc, *Geology*, 19, 881–884, 1991a.
- McCaffrey, R., Earthquakes and ophiolite emplacement in the Molucca Sea collision zone, Indonesia, *Tectonics*, 10, 433–453, 1991b.
- McCaffrey, R., and G. A. Abers, Orogeny in arc-continent collision: The Banda arc and western New Guinea, *Geology*, 19, 563–566, 1991.
- McCaffrey, R., and J. Nabelek, The geometry of back arc thrusting along the eastern Sunda arc, Indonesia: Constraints from earthquake and gravity data, *J. Geophys. Res.*, 89, 6171–6179, 1984.
- McCaffrey, R., P. Zwick, Y. Bock, L. Prawirodirdjo, J. Genrich, S. S. O. Puntodewo, and C. Subarya, Strain partitioning during oblique plate convergence in northern Sumatra: Geodetic and seismologic constraints and numerical modeling, *J. Geophys. Res.*, 105, 28,363–28,376, 2000.
- McKenzie, D., and J. Jackson, The relationship between strain rates, crustal thickening, palaeomagnetism, finite strain and fault movements within a deforming zone, *Earth Planet. Sci. Lett.*, 65, 182–202, 1983.
- Michel, G. W., et al., Crustal motion and block behaviour in SE-Asia from GPS measurements, *Earth Planet. Sci. Lett.*, 187, 239–244, 2001.
- Milsom, J., D. Masson, G. Nichols, N. Sikumbang, B. Dwiyanto, L. Parson, and H. Kallagher, The Manokwari trough and the western end of the New Guinea trench, *Tectonics*, 11, 145–153, 1992.
- Milsom, J., S. Kaye, and Sardjono, Extension, collision and curvature in the eastern Banda arc, *Geol. Soc. Spec. Publ.*, 106, 85–94, 1996.
- Molnar, P., and D. Gray, Subduction of continental lithosphere: Some constraints and uncertainties, *Geology*, 7, 58–62, 1979.
- Molnar, P., and P. Tapponnier, Cenozoic tectonics of Asia: Effects of a continental collision, *Science*, 189, 419–426, 1975.
- Newcomb, K. R., and W. R. McCann, Seismic history and seismotectonics of the Sunda Arc, *J. Geophys. Res.*, 92, 421–439, 1987.
- Nikolaidis, R., Observation of geodetic and seismic deformation with the Global Positioning System, Ph.D. thesis, Univ. of Calif., San Diego, Calif., 2002.
- Okal, E. A., Historical seismicity and seismotectonic context of the great 1979 Yapen and Biak, Irian Jaya earthquakes, *Pure Appl. Geophys.*, 154, 633–675, 1999.
- Prawirodirdjo, L., et al., Geodetic observations of interseismic strain segmentation at the Sumatra subduction zone, *Geophys. Res. Lett.*, 24, 2601–2604, 1997.
- Prawirodirdjo, L., Y. Bock, J. F. Genrich, S. S. O. Puntodewo, J. Rais, C. Subarya, and S. Sutisna, One century of tectonic deformation along the Sumatran fault from triangulation and GPS surveys, *J. Geophys. Res.*, 105, 28,343–28,361, 2000.
- Puntodewo, S. S. O., et al., GPS measurements of crustal deformation within the Pacific-Australia plate boundary zone in Irian Jaya, Indonesia, *Tectonophysics*, 237, 141–153, 1994.
- Sella, G. F., T. H. Dixon, and A. Mao, REVEL: A model for recent plate velocities from space geodesy, *J. Geophys. Res.*, 107(B4), 2081, doi:10.1029/2000JB000033, 2002.
- Seno, T., and D. E. Kaplan, Seismotectonics of western New Guinea, *J. Phys. Earth*, 36, 107–124, 1988.
- Sieh, K., and D. Natawidjaja, Neotectonics of the Sumatran fault, Indonesia, *J. Geophys. Res.*, 105, 28,295–28,326, 2000.
- Sieh, K., J. Rais, and Y. Bock, Neotectonic and paleoseismic studies in West and North Sumatra, *Eos Trans. AGU*, 72, 460, 1991.
- Sieh, K., J. Zachariassen, Y. Bock, L. Edwards, F. Taylor, and P. Gans, Active tectonics of Sumatra, *Geol. Soc. Am. Abstr. Programs*, 26, A-382, 1994.
- Simons, W. J. F., et al., Observing plate motions in SE Asia: Geodetic results of the GEODYSSSEA project, *Geophys. Res. Lett.*, 26, 2081–2084, 1999.
- Smith, W., and D. Sandwell, Global sea floor topography from satellite altimetry and ship depth soundings, *Science*, 277, 1956–1962, 1997.
- Stevens, C. R., R. McCaffrey, Y. Bock, J. F. Genrich, Endang, C. Subarya, S. S. O. Puntodewo, Fauzi, and C. Vigny, Rapid rotations about a vertical axis in a collisional setting revealed by the Palu fault, Sulawesi, Indonesia, *Geophys. Res. Lett.*, 26, 2677–2680, 1999.
- Stevens, C. W., GPS studies of crustal deformation and earthquakes in Indonesia and Papua New Guinea, Ph.D. thesis, Rensselaer Polytech. Inst., Troy, N. Y., 1999.
- Stevens, C. W., M. Pubellier, R. McCaffrey, Y. Bock, J. Genrich, and C. Subarya, Evidence for block rotations and basal shear in the world's fastest slipping continental shear zone in NW New Guinea, in *Plate Boundary Zones, Geodyn. Ser.*, vol. 30, edited by S. Stein and J. Freymueller, pp. 87–99, AGU, Washington, D. C., 2002.
- Thatcher, W., Microplate versus continuum descriptions of active tectonic deformation, *J. Geophys. Res.*, 100, 3885–3894, 1995.
- Tregoning, P., Plate kinematics in the western Pacific derived from geodetic observations, *J. Geophys. Res.*, 107(B1), 2020, doi:10.1029/2001JB000406, 2002.
- Tregoning, P., F. K. Brunner, Y. Bock, S. S. O. Puntodewo, R. McCaffrey, J. F. Genrich, E. Calais, J. Rais, and C. Subarya, First geodetic measure-

- ment of convergence across the Java Trench, *Geophys. Res. Lett.*, *21*, 2135–2138, 1994.
- Untung, M., N. Buyung, E. Kertapati, Undang, and C. R. Allen, Rupture along the Great Sumatran Fault, Indonesia, during the earthquakes of 1926 and 1943, *Bull. Seismol. Soc. Am.*, *75*, 313–317, 1985.
- Walpersdorf, A., C. Rangin, and C. Vigny, GPS compared to long-term geologic motion of the north arm of Sulawesi, *Earth Planet. Sci. Lett.*, *159*, 47–55, 1998.
- Wessel, P., and W. H. F. Smith, Free software helps map and display data, *Eos Trans. AGU*, *72*, 441, 1991.
- Williams, S. D. P., The effect of coloured noise on the uncertainties of rates estimated from geodetic time series, *J. Geod.*, *76*, 483–494, 2003.
- Zhang, J., Y. Bock, H. Johnson, P. Fang, S. Williams, J. F. Genrich, S. Wdowinski, and J. Behr, Southern California permanent GPS geodetic array: Error analysis of daily position estimates and site velocities, *J. Geophys. Res.*, *102*, 18,035–18,055, 1997.
-
- Y. Bock, J. F. Genrich, and L. Prawirodirdjo, Cecil H. and Ida M. Green Institute of Geophysics and Planetary Physics, Scripps Institution of Oceanography, La Jolla, CA 92093-0225, USA. (ybock@ucsd.edu)
- E. Calais, Department of Earth and Atmospheric Sciences, Purdue University, West Lafayette, IN 47907, USA.
- R. McCaffrey and C. W. Stevens, Department of Earth and Environmental Sciences, Rensselaer Polytechnic Institute, Troy, NY 12180, USA.
- S. S. O. Puntodewo and C. Subarya, National Coordination Agency for Surveying and Mapping, Cibinong 16911, Indonesia.

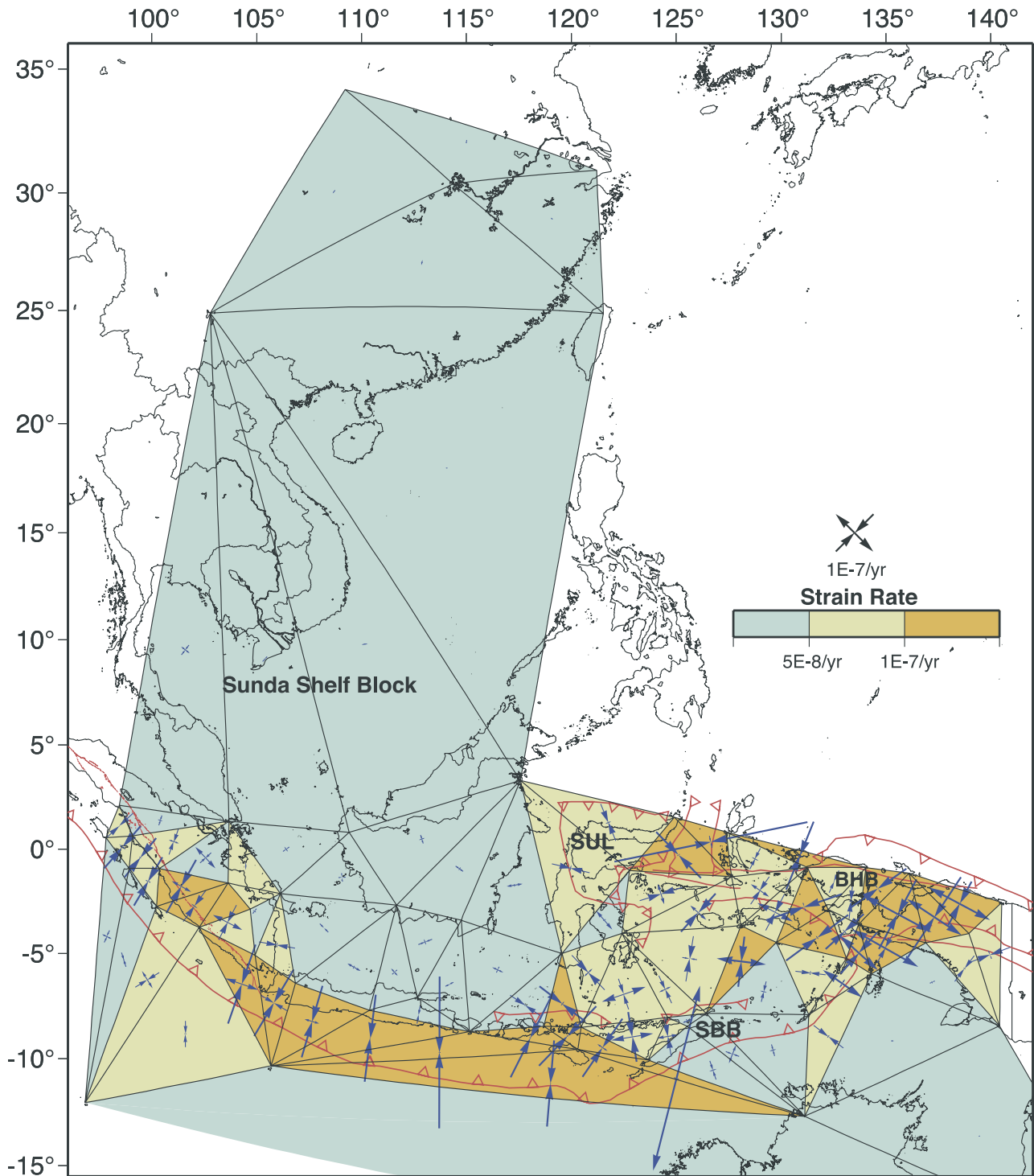


Figure 9. Principal surface strain rates (dark blue arrows indicating contraction/extension) computed for triangular elements (boundaries indicated by solid lines) with nodes located at GPS stations. Elements are shaded light green for corresponding strain rates smaller than 5×10^{-8} per year, yellow for rates between 5×10^{-8} and 10^{-7} per year, and mustard colored for rates exceeding 10^{-7} per year. Red lines trace faults. SUL, East Sulawesi Block; BHB, Bird's Head Block; SBB, South Banda Block.